

A posteriori error estimation of hierarchical type for the Schrödinger operator with inverse square potential

Hengguang Li · Jeffrey S. Ovall

Received: 5 June 2013 / Revised: 23 January 2014 / Published online: 22 April 2014
© Springer-Verlag Berlin Heidelberg 2014

Abstract We develop an a posteriori error estimate for mixed boundary value problems of the form $(-\Delta + \mathcal{V})u = f$, where the potential \mathcal{V} may possess inverse-square singularities at finitely many points in the domain. We prove that our error estimate can be efficiently computed and is asymptotically identical to the actual error in the energy norm, on a family of geometrically graded meshes appropriate for singular solutions of such problems. Therefore, our estimate can be used for a practical stopping criterion. A variety of numerical experiments support our theoretical results. We also offer a direct convergence and effectivity comparison between the geometrically-graded meshes, which are based on a priori knowledge of possible singularities in the solution, and adaptively refined meshes driven by local error indicators associated with our a posteriori error estimate.

Mathematics Subject Classification 65N15 · 65N30 · 65N50

H. Li was partially supported by the NSF Grant DMS-1158839. J.S. Ovall was partially supported by the NSF Grant DMS-1216672.

H. Li
Department of Mathematics, Wayne State University, Detroit, MI 48202, USA
e-mail: hli@math.wayne.edu

J. S. Ovall (✉)
Fariborz Maseeh Department of Mathematics and Statistics, Portland State University,
Portland, OR 97201, USA
e-mail: jovall@pdx.edu

1 Introduction

We consider mixed boundary value problems associated with the Schrödinger operator

$$Hu := (-\Delta + \mathcal{V})u$$

in a 2D polygonal domain Ω , where the potential function \mathcal{V} may have singularities of the type $|x - y_i|^{-2}$ for a finite set of points $\{y_i\} \subset \overline{\Omega}$ —this is known as a centrifugal, or inverse square, potential. Such potentials are significant in quantum mechanics (for example, see [26, 27, 43, 52]), and require special analysis for well-posedness and regularity results as well as for the development of effective numerical algorithms. Note that due to the singular potential, this equation is naturally studied in weighted Sobolev spaces instead of the usual Sobolev space H^1 (for example, see [25, 26, 32, 41] and references therein).

The non-smooth behavior of the potential near a singular point y_i may also cause local singularities in the solution. These singularities, together with those due to corners in the domain and changes in the type of boundary condition, must be given special attention in order to achieve desired finite element approximation properties. Based on a priori estimates in suitable weighted Sobolev spaces, a systematic construction of graded meshes has been proposed in [41] to yield finite element solutions with the optimal order of convergence in the presence of such singularities in the solution (see [33] for a similar treatment in 3D). Such graded meshes have also proven to be effective in other situations in which singular solutions are known to arise [7, 16, 17, 39, 46]. These graded meshes are generated using a recursive process, giving rise to families of nested shape-regular triangulations; the constant of shape-regularity for the family is controlled by the strength of the grading, which is fixed for a given problem.

We are aware of no contributions concerning a posteriori error estimates for such problems. This may be due to the fact that a posteriori error estimates are most commonly associated with automatic adaptive refinement driven by related local error indicators, whereas those accustomed to working in weighted Sobolev spaces generally prefer graded meshes which can be more closely tied to the weighting in these spaces. However, regardless of the general meshing approach, any practical algorithm should have an efficient and reliable mechanism for determining when an approximation adequately resolves the solution. The singularity(ies) in the potential \mathcal{V} pose challenges in selection and analysis of appropriate error estimates, so error estimates developed for standard elliptic problems may not work at all without significant modification, or will at least require a different sort of analysis. For example, residual-based error estimates for standard elliptic problems (cf. [2]) involve the L^2 -norm of the strong form of the residual on each element, but in this case that residual is not in L^2 near the singular points of \mathcal{V} . One also quickly sees that the popular gradient recovery schemes, such as those surveyed in [53], are not designed to address the term $\mathcal{V}u$.

Error estimates of hierarchical type, which are based on the computation of an approximate error function in an auxiliary space, have a long and successful history in finite element computations [4, 8, 11, 12, 15, 22, 31, 45], at least for standard elliptic problems. Often in practice, such an approximate error function can be used quite flexibly in terms of error estimation in a variety of measures, and for adaptivity with

respect to a variety of objectives [34,44,45]. We here analyze a hierarchical error estimate, arguing that it is asymptotically identical to the actual error in the energy norm

$$\frac{\|\varepsilon_n\|}{\|u - u_n\|} \rightarrow 1. \quad (1)$$

Because the approximate error function ε_n is a global Galerkin projection of the error $u - u_n$ onto an auxiliary space, we argue that the system for computing this projection is well-conditioned—in contrast to that for computing u_n . As a matter of practical interest, we also include numerical results for adaptively refined meshes based on local error indicators associated with our a posteriori error estimates, demonstrating that they provide very similar performance to the graded meshes for which we have proven asymptotic exactness. The adaptive algorithm used for these experiments uses the Hessian of ε_n as part of a more aggressive refinement scheme than is often employed in other codes, so we provide numerical evidence that the Hessian of ε_n approximates of the Hessian of u .

To simplify the presentation, we shall focus on the linear finite element approximation of a model problem (2) in which \mathcal{V} possesses a single inverse-square singularity at the origin. However, we take care to outline the arguments in such a way that extensions to multiple singularities should be obvious, and we highlight certain aspects of these extensions in several places. Some of the results extend quite readily to higher-order elements as well, but others would require further technical arguments and practical implementation issues which we choose to pursue in later work. Note that our a posteriori estimates naturally hold on optimal graded meshes for the usual geometric corner singularities in the solution, which is the special case when the potential function \mathcal{V} is smooth.

The rest of the paper is organized as follows. In Sect. 2, we describe our model problem and the necessary function spaces and norms required to properly discuss well-posedness and regularity. Section 3 includes basic geometric properties of the finite element spaces and related estimates which lead to the aforementioned spectral equivalence result (Theorem 3.6), as well as the definition of the graded meshes and optimal-order a priori convergence rates even in the case of solutions with singularities (Theorem 3.9). Section 4 contains the proof of (1), which exploits mesh symmetries throughout much of the domain for essential super-convergence results. A variety of numerical experiments, which convincingly illustrate our convergence and effectivity assertions, are given in Sect. 5. Also in this section are numerical comparisons between the graded meshes and adaptive meshes, as well as a few results on how the approximate error function can be used to recover higher-order derivative information about the solution.

2 The model problem and basic definitions

2.1 The model problem

Given a bounded domain $\Omega \subset \mathbb{R}^2$, which we assume to be polygonal for convenience, we consider the model problem of finding u in a suitable function space $\mathcal{H} \subset H^1(\Omega)$ such that

$$(-\Delta + \delta r^{-2})u = f \text{ in } \Omega, \quad u = 0 \text{ on } \partial\Omega_D, \quad \partial_\nu u = 0 \text{ on } \partial\Omega_N \tag{2}$$

in a weak sense. Here $\delta > 0$ is constant, and $r = r(x) = |x|$ is the distance to the origin, which is assumed to be in $\bar{\Omega}$. The boundary $\partial\Omega$ is disjointly partitioned into Dirichlet and Neumann portions, $\partial\Omega_D$ and $\partial\Omega_N$, with the assumption that Neumann boundary conditions are not allowed on adjacent edges of a vertex on $\partial\Omega$ unless that vertex is the origin.

We use standard notation for (real) Hilbert spaces, norms and semi-norms

$$H^m(\Omega) = \{v \in L^2(\Omega) : \partial^\alpha v \in L^2(\Omega) \text{ for all } |\alpha| \leq m\},$$

$$\|v\|_m = \left(\sum_{|\alpha| \leq m} \|\partial^\alpha v\|_{L^2(\Omega)}^2 \right)^{1/2}, \quad |v|_m = \left(\sum_{|\alpha|=m} \|\partial^\alpha v\|_{L^2(\Omega)}^2 \right)^{1/2},$$

with multi-index $\alpha = (\alpha_1, \alpha_2) \in \mathbb{Z}_{\geq 0}^2$ and $|\alpha| = \alpha_1 + \alpha_2$, where $\|v\|_{L^2(\Omega)}^2 = \|v\|_0^2 = \int_\Omega v^2 dx$. We also use the notation $\|v\|_{m,\omega}$ and $|v|_{m,\omega}$ for $\omega \subset \Omega$, when $\|\partial^\alpha v\|_{L^2(\omega)}$ is used above in place of $\|\partial^\alpha v\|_{L^2(\Omega)}$. In a few places, we use the more general Sobolev spaces $W^{k,p}$ and their norms, and refer the reader to [1] for their definitions and imbedding properties.

The differential operator in (2) is typical of a more general class of Schrödinger operators, which we now describe. Let P be the set composed of vertices (corners) of the domain Ω and the points on the boundary $\partial\Omega$ where the boundary condition switches from the Dirichlet to Neumann or vice versa. Let $Q \subset \bar{\Omega}$ be a fixed finite set of points, and define $R(x) = \prod_{y \in Q} |x - y|^2$. Namely, in the neighborhood of each $y \in Q$, $R(x)$ is comparable with the square of the distance to y . Let $\mathcal{V} : \bar{\Omega} \setminus Q \rightarrow \mathbb{R}$ be a function such that $R\mathcal{V}$ may be extended to a smooth function on $\bar{\Omega}$. Namely, \mathcal{V} may be an inverse square potential, with $\mathcal{V} = \delta r^{-2}$ as a simple example. The more general type of the problem is

$$(-\Delta + \mathcal{V})u = f \text{ in } \Omega, \quad u = 0 \text{ on } \partial\Omega_D, \quad \partial_\nu u = 0 \text{ on } \partial\Omega_N. \tag{3}$$

Denote by $S := P \cup Q$, the set composed of the vertices of the domain Ω , points where the boundary condition switches types, and the singular points of the potential \mathcal{V} . In particular, for the model problem (2), P is the set containing all vertices of Ω and points where the boundary condition changes type, and $Q = \{\mathbf{0}\}$. Note that even in the case when \mathcal{V} is smooth on $\bar{\Omega}$, it is well known that the weak solution of (3) generally possesses singularities at corners of Ω as well as points at which the boundary condition switches type (cf. [3,5,7,21,28,29,35–37,40,51]). Although, for sake of clarity in exposition, we will focus on the model problem (2), our results extend to the more general problems (3), and we highlight at several key points how such extensions can be made.

Well-posedness and regularity results for such problems are given in [41] in terms of the following weighted Sobolev spaces and their corresponding norms

$$\mathcal{K}_a^m(\Omega) = \{v \in L^2(\Omega) : \vartheta^{|\alpha|-a} \partial^\alpha v \in L^2(\Omega) \text{ for all } |\alpha| \leq m\}, \tag{4}$$

$$|v|_{\mathcal{K}_a^m} = \left(\sum_{|\alpha|=m} \|\vartheta^{m-a} \partial^\alpha v\|_{L^2(\Omega)}^2 \right)^{1/2}, \quad \|v\|_{\mathcal{K}_a^m}^2 = \left(\sum_{|\alpha| \leq m} |v|_{\mathcal{K}_a^m}^2 \right)^{1/2},$$

where $\vartheta(x)$ is the distance from x to the set S . Note that $S = P \cup Q$ includes other points different from the origin and ϑ is equivalent to r near the origin. As with the standard (unweighted) norms and seminorms, we define $\|v\|_{\mathcal{K}_a^m(\omega)}$ and $|v|_{\mathcal{K}_a^m(\omega)}$ on subdomains $\omega \subset \Omega$ in the obvious way.

2.2 Regularity results

We henceforth focus on the weak form of (2): Find $u \in \mathcal{H}$ such that

$$B(u, v) := \int_{\Omega} \nabla u \cdot \nabla v + \delta r^{-2} uv \, dx = \int_{\Omega} f v \, dx := F(v), \quad \forall v \in \mathcal{H}. \tag{5}$$

The natural Hilbert space \mathcal{H} for this variational problem is

$$\mathcal{H} = \{u \in \mathcal{K}_1^1(\Omega) : u = 0 \text{ on } \partial\Omega_D\}. \tag{6}$$

It is clear from its definition that $\mathcal{K}_1^1(\Omega) \subset H^1(\Omega)$. The associated bilinear form B is an inner-product in this case, and we denote the corresponding ‘‘energy’’-norm by $\| \cdot \|$, so $\|v\|^2 := B(v, v)$. As before, we use $\| \cdot \|_{\omega}$ when the associated integral is restricted to $\omega \subset \Omega$.

We first establish the equivalence of the energy-norm and the \mathcal{K}_1^1 -norm.

Lemma 2.1 *For any function $v \in \mathcal{H}$, the energy-norm and the \mathcal{K}_1^1 -norm are equivalent. Namely, there is a constant $C > 0$, independent of v , such that*

$$C^{-1} \|v\| \leq \|v\|_{\mathcal{K}_1^1(\Omega)} \leq C \|v\|.$$

Proof Recalling the definitions of r and ϑ and the roles they play in both norms, we see that we need only compare the norms in the immediate neighborhoods of boundary points in P . In these regions, by the local Poincaré inequality in polar coordinates, it is well known that the L^2 -norm of $\vartheta^{-1}v$ is bounded by the H^1 -seminorm of v (see [6, 36, 37] and Lemma 3.1 in [41]). This completes the proof. \square

Remark 2.2 The use of local Poincaré inequalities in the neighborhood of a point in P requires the Dirichlet boundary condition on at least one edge adjacent to the point. This is the reason that we assume no adjacent Neumann boundary condition is allowed for a point in P . Although it can be removed if we enlarge these weighted spaces as in [40], this assumption is maintained in order to simplify the presentation.

In addition to the norm equivalence, Lemma 2.1 leads to the well-posedness of (5) in \mathcal{H} . Furthermore, the following regularity result is proven in [41, Theorem 3.3]:

Theorem 2.3 *There is a constant $\eta > 0$, such that the solution u of Eq. (5) satisfies the following regularity estimate:*

$$\|u\|_{\mathcal{K}_{a+1}^{m+1}(\Omega)} \leq C \|f\|_{\mathcal{K}_{a-1}^{m-1}(\Omega)}, \tag{7}$$

for any $0 \leq a < \eta$, where the constant C is independent of f and u .

Remark 2.4 To be more precise, the regularity estimate (7) holds in a neighborhood of each singular point $z \in S$, with the constant (local regularity index) η_z chosen to be the smallest eigenvalue of the local operator pencil near z (see [35,37] and [41, Equations (20) and (21)]). We then take the global regularity index in Theorem 2.3 to be $\eta = \min\{\eta_z : z \in S\}$. A thorough discussion of how to obtain local and global regularity indices for problems of the sort described here can be found in [41].

The a priori results (Lemma 2.1 and Theorem 2.3) will be used to obtain finite element estimates on graded meshes in Sects. 3 and 4.

3 Discretization and basic results

In this section, we formulate the finite element approximation for the Schrödinger-type equation (2). We shall introduce a systematic construction of graded meshes that yield finite element solutions with the optimal rate of convergence, although the solution may present singularities near the origin and near the vertices of Ω . Several useful properties of the finite element functions will be investigated in preparation for our a posteriori estimate in Sect. 4.

3.1 Triangulation and finite element spaces

Given a triangulation \mathcal{T} of Ω , let \mathcal{V} be the vertex set (the vertices of all triangles) and let \mathcal{E} be the edge set. We implicitly assume that \mathcal{V} includes all the singular points in S . We define the two spaces

$$V = V(\mathcal{T}) = \{\mathcal{H} \cap C(\bar{\Omega}) : v|_T \in \mathbb{P}_1, \forall T \in \mathcal{T}\}, \tag{8}$$

$$W = W(\mathcal{T}) = \{\mathcal{H} \cap C(\bar{\Omega}) : v|_T \in \mathbb{P}_2, \forall T \in \mathcal{T} \text{ and } v(z) = 0, \forall z \in \mathcal{V}\}. \tag{9}$$

The space \mathbb{P}_k consists of polynomials of total degree k or less. We note that it is necessary that $v(0) = 0$ for $v \in V$; if \mathcal{V} includes several singularities of type $|x - y|^{-2}$ for $y \in \bar{\Omega}$, it would be necessary that $v(y) = 0$ for each of them. We will approximate the solution of (5) in the space V and assess the error of this approximation in the space W .

For each vertex $z \in \mathcal{V}$ we define the continuous, piecewise-linear function ℓ_z which satisfies the Kronecker property $\ell_z(z') = \delta_{zz'}$ for all $z, z' \in \mathcal{V}$. It is clear that these functions form a (non-smooth) partition of unity for Ω , $\sum_{z \in \mathcal{V}} \ell_z = 1$. For each edge $e \in \mathcal{E}$ we define the continuous, piecewise quadratic function $b_e = 4\ell_z\ell_{z'}$, where $z, z' \in \mathcal{V}$ are the endpoints of e ; the factor of four is merely to make $b_e(m_e) = 1$,

where m_e is the midpoint of e . Let $\mathcal{V}^\circ = \mathcal{V} \setminus (\{0\} \cup \partial\Omega_D)$ and $\mathcal{E}^\circ = \mathcal{E} \setminus \partial\Omega_D$. It is apparent that

$$V = \text{span}\{\ell_z : z \in \mathcal{V}^\circ\}, \quad W = \text{span}\{b_e : e \in \mathcal{E}^\circ\},$$

and these sets are bases for their respective spaces. We also assume that, for any $z \in \mathcal{V}^s = \mathcal{V} \setminus \mathcal{V}^\circ$, there is $z' \in \mathcal{V}^\circ$ which shares an edge with z .

In the following lemma we collect a few basic results concerning the basis functions and the geometry of the mesh \mathcal{T} . Many of these can be found in [30], for example, and are here stated without proof.

Lemma 3.1 *Let $T \in \mathcal{T}$ have vertices z_k , with internal angles $\theta_k, k = 1, 2, 3$. Let $\ell_k \in \mathbb{P}_1$ satisfy $\ell_k(z_j) = \delta_{jk}$, and take $b_k = 4\ell_{k-1}\ell_{k+1}$, where the indices are understood modulo 3 (i.e. $b_4 = b_1, b_0 = b_3$). The following hold:*

$$\ell_k(x) = \nabla \ell_k \cdot (x - z_{k-1}) = \nabla \ell_k \cdot (x - z_{k+1}); \tag{10}$$

$$\nabla \ell_k \cdot \nabla \ell_k = \frac{\cot \theta_{k-1} + \cot \theta_{k+1}}{2|T|} \quad \text{and} \quad \nabla \ell_{k-1} \cdot \nabla \ell_{k+1} = -\frac{\cot \theta_k}{2|T|}; \tag{11}$$

$$\int_T \ell_1^p \ell_2^q \ell_3^r dx = \frac{2|T| p! q! r!}{(p + q + r + 2)!} \quad \text{for } p, q, r \in \mathbb{Z}_{\geq 0}; \tag{12}$$

$$\int_T \nabla b_k \cdot \nabla b_k dx = \frac{4}{3}(\cot \theta_{k-1} + \cot \theta_k + \cot \theta_{k+1}); \tag{13}$$

$$\int_T \nabla b_{k-1} \cdot \nabla b_{k+1} dx = -\frac{4}{3} \cot \theta_k. \tag{14}$$

Consequently, the following norm equivalence holds for functions in W .

Lemma 3.2 *Let $w \in W = W(\mathcal{T})$ be given and consider a triangle $T \in \mathcal{T}$. There is a constant C , depending only on the angles in \mathcal{T} , such that*

$$\|r^{-1}w\|_{0,T} \leq C|w|_{1,T}.$$

Proof On T , $w = w_1b_1 + w_2b_2 + w_3b_3$. Therefore we have the obvious correspondence between $w|_T$ and $\mathbf{w} = (w_1, w_2, w_3)^t \in \mathbb{R}^3$. It holds that

$$\|r^{-1}w\|_{0,T}^2 = \mathbf{w}^t K \mathbf{w} \quad \text{and} \quad |w|_{1,T}^2 = \mathbf{w}^t A \mathbf{w},$$

where $K_{ij} = \int_T r^{-2}b_j b_i dx$ and $A_{ij} = \int_T \nabla b_j \cdot \nabla b_i dx$. It is clear from their definitions that K and A are symmetric positive definite, and we deduce that

$$\|r^{-1}w\|_{0,T}^2 \leq \frac{\lambda_{\max}(K)}{\lambda_{\min}(A)} |w|_{1,T}^2.$$

The eigenvalues of A are given in [30] as

$$\lambda_k(A) = \frac{4}{3} \left(c_1 + c_2 + c_3 - 2\sqrt{\frac{c_1^2 + c_2^2 + c_3^2}{3}} \cos\left(\frac{\psi + 2(k-1)\pi}{3}\right) \right), \tag{15}$$

$$\psi = \arccos\left(\frac{3\sqrt{3}c_1c_2c_3}{(c_1^2 + c_2^2 + c_3^2)^{3/2}}\right), \quad c_j = \cot \theta_j, \tag{16}$$

and it holds that $0 < \lambda_1 \leq \lambda_3 \leq \lambda_2$. So it remains to bound the largest eigenvalue of K .

Letting z be the point on ∂T which is closest to the origin, we have $r = |x| \geq |x - z|$ for $x \in T$. It is clear that

$$\int_T r^{-2}b_k^2 dx \leq \int_T |x - z|^{-2}b_k^2 dx,$$

for the three quadratic edge-bump functions b_k associated with this triangle. We first consider the case that z is a vertex of T . Without loss of generality, we call it z_1 and number the other vertices arbitrarily. Using the definition of b_k , and (10)–(12), we deduce that

$$\int_T |x - z_1|^{-2}b_1^2 dx \leq \frac{4}{3}(c_1 + c_2) \quad \text{and} \quad \int_T |x - z_1|^{-2}b_1^2 dx \leq \frac{4}{3}(c_1 + c_3). \tag{17}$$

The first of these results can be seen as follows:

$$\begin{aligned} \int_T |x - z_1|^{-2}b_1^2 dx &= 16 \int_T \left(\nabla \ell_3 \cdot \frac{(x - z_1)}{|x - z_1|} \right)^2 \ell_2^2 dx \leq 16|\nabla \ell_3|^2 \int_T \ell_2^2 dx \\ &= 16 \frac{c_1 + c_2}{2|T|} \frac{2|T|2!}{4!} = \frac{4}{3}(c_1 + c_2). \end{aligned}$$

Analogous arguments yield

$$\int_T |x - z_1|^{-2}b_2^2 dx \leq \frac{4}{3}(c_1 + c_2) \quad \text{and} \quad \int_T |x - z_1|^{-2}b_3^2 dx \leq \frac{4}{3}(c_1 + c_3). \tag{18}$$

So

$$\text{trace}(K) = \sum_{k=1}^3 \int_T r^{-2}b_k^2 dx \leq \sum_{k=1}^3 \int_T |x - z_1|^{-2}b_k^2 dx \leq 4c_1 + 2c_2 + 2c_3.$$

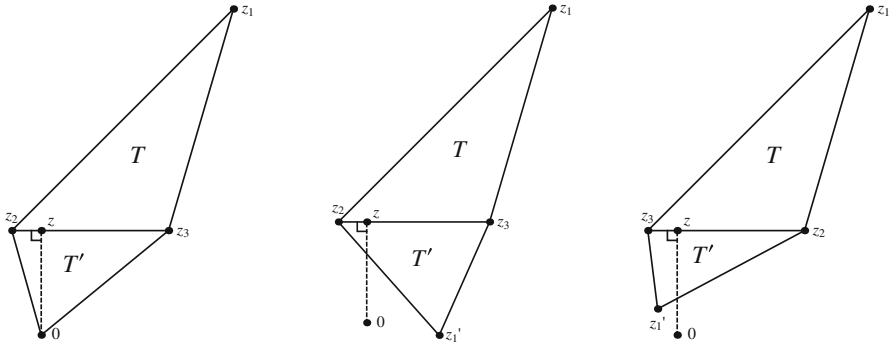


Fig. 1 Typical configurations for the proof of Lemma 3.2

Since $\lambda_{\max}(K) < \text{trace}(K)$, it is clear that $\lambda_{\max}(K)/\lambda_{\min}(A)$ can be bounded above by a scale-invariant constant which depends only on the angles of T , and we may take C to be the square-root of any such constant.

We now consider the case where z is not a vertex of T . Without loss of generality, we take z_1 to be the vertex opposite the edge e on which z lies, and let T' be the triangle adjacent to T across the e . We denote by z'_1 the vertex of T' opposite e . It is always possible to label the endpoints z_2, z_3 of e in such a way that $\angle 0z_2z_3$ is not smaller than $\angle z'_1z_2z_3$ (see Fig. 1). We determine from (10) (or directly) that $\ell_1 = (x - z) \cdot \nabla \ell_1$. Using the same type of arguments as above, we determine that

$$\text{trace}(K) \leq \int_T r^{-2} b_1^2 dx + \frac{8}{3}(c_2 + c_3).$$

Taking $\phi = \phi(x)$ to be the angle $\angle 0z_2x$ for $x \in T \setminus \{z_2\}$, we have, by the Law of Cosines,

$$|x|^2 = |x - z_2|^2 + |z_2|^2 - 2|x - z_2||z_2| \cos \phi.$$

If $\phi \geq \pi/2$, it is clear that $|x| > |x - z_2|$. Now suppose that $\phi < \pi/2$. If $\psi = \psi(T')$ is the smallest angle in T' , then $\phi \geq \psi$. From this we deduce that

$$|x|^2 \geq (1 - \cos^2 \phi)|x - z_2|^2 \geq (1 - \cos^2 \psi)|x - z_2|^2.$$

In any case, we see that $|x| \geq \sqrt{1 - \cos^2 \psi}|x - z_2|$, for any $x \in T$. Finally, we see that

$$\int_T r^{-2} b_1^2 dx \leq (1 - \cos^2 \psi)^{-1} \int_T |x - z_2|^{-2} b_1^2 dx.$$

It is clear from the arguments above that this final quantity is bounded by a constant depending only on the angles of T and T' . The rest of the argument follows as it did for the case when z was a vertex of T . This completes the proof. \square

As an immediate corollary, we have

Corollary 3.3 *There is a constant C , depending only on the angles in \mathcal{T} , such that*

$$\|w\|^2 \leq (1 + \delta C)|w|_1^2$$

for all $w \in W(\mathcal{T})$, where $\delta > 0$ is as in the differential operator (2).

Remark 3.4 Although Lemma 3.2 was proven for $r = |x|$, it is clear from the argument the result holds for $r = |x - y|$, where $y \in \mathcal{V}$. Furthermore, it is evident that, if $\mathcal{V}(x)$ has the form $\delta_1|x - y_1|^{-2} + \dots + \delta_m|x - y_m|^{-2}$, where $\delta_k > 0$ is constant and $y_k \in \mathcal{V}$, then we have a result analogous to Corollary 3.3. Specifically, if $B(\cdot, \cdot)$ is the bilinear form associated with $-\Delta + \mathcal{V}$, and $\|\cdot\|$ is the associated energy-norm, then $\|w\|^2 \leq (1 + (\delta_1 + \dots + \delta_m)C)|w|_1^2$ for all $w \in W(\mathcal{T})$.

Recalling that $\vartheta(x)$ is the distance between x and the singular set S , and noting that $\vartheta(x) \sim |x - y|$ for x “near” $y \in S$, the proof of Lemma 3.2 is readily adjusted to accommodate ϑ , rather than $r = |x - y|$ for each $y \in \mathcal{Q}$. We formally state its analogue, which will be used in later results.

Lemma 3.5 *Let $w \in W = W(\mathcal{T})$ be given, and consider $T \in \mathcal{T}$. There is a constant C , depending only on the angles in \mathcal{T} and the number of singular points in S , such that*

$$\|\vartheta^{-1}w\|_{0,T} \leq C|w|_{1,T}.$$

3.2 The approximation and error estimation equations

We now introduce the finite element solution for the Schrödinger equation and the associated error estimation equation for our a posteriori estimates.

In Definition 3.7 below we shall describe a family of nested, graded meshes \mathcal{T}_n which are appropriate for resolving solutions of (5) in the spaces $V_n = V(\mathcal{T}_n)$. More specifically, we consider the family of *approximation problems*: Find $u_n \in V_n$ such that

$$B(u_n, v_n) = F(v_n), \quad \forall v_n \in V_n. \tag{19}$$

We will also consider the associated family of *error estimation problems*: Find $\varepsilon_n \in W_n = W(\mathcal{T}_n)$ such that

$$B(\varepsilon_n, w_n) = F(w_n) - B(u_n, w_n) = B(u - u_n, w_n), \quad \forall w_n \in W_n. \tag{20}$$

By Lemma 2.1, $B(\cdot, \cdot)$ is an inner-product. Thus, we see that ε_n is the orthogonal projection of the error $u - u_n$ onto the space W_n with respect to $B(\cdot, \cdot)$.

In Sect. 4, we investigate the relevant estimation properties of the approximate error function ε_n . Because the computation of ε_n involves the solution of a linear system

which is larger than that for computing u_n , we argue that this is far less costly than it might initially appear. We do so by proving that the stiffness matrix associated with (20) is spectrally-equivalent to its diagonal, making the linear system solvable by simple means; a couple of steps of Jacobi-preconditioned conjugate gradient (CG) is sufficient, for example. In contrast, the condition number of the stiffness matrix associated with (19) grows without bound as the mesh is refined, and therefore requires more sophisticated solution techniques; we use (algebraic) multigrid with an incomplete LU smoother [13] as a preconditioner for CG.

The spectral equivalence result for the stiffness matrix associated with (20) is stated as follows.

Theorem 3.6 *Let $\{b_i : 1 \leq i \leq N\}$ be an enumeration of the basis for $W = W(\mathcal{T})$ and define $\mathcal{B} \in \mathbb{R}^{N \times N}$ by $\mathcal{B}_{ij} = B(b_i, b_j)$. Then \mathcal{B} is spectrally-equivalent to its diagonal.*

Proof Let $\mathbf{w} \in \mathbb{R}^N$ be the coefficient vector of $w \in W$ with respect to the (ordered) basis. Then $\mathbf{w}^t \mathcal{B} \mathbf{w} = \|w\|^2$. By Corollary 3.3, we see that $|w|_1^2 \leq \|w\|^2 \leq (1 + \delta C)|w|_1^2$. Therefore,

$$\mathbf{w}^t A \mathbf{w} \leq \mathbf{w}^t \mathcal{B} \mathbf{w} \leq (1 + \delta C) \mathbf{w}^t A \mathbf{w} \quad \text{for all } \mathbf{w} \in \mathbb{R}^N,$$

where $A_{ij} = \int_{\Omega} \nabla b_j \cdot \nabla b_i \, dx$. So A and \mathcal{B} are spectrally-equivalent, as are their diagonals. In [10] (see also [8,31]) we have argued that A is spectrally-equivalent to its diagonal, which implies that \mathcal{B} is as well. □

3.3 A priori error bounds on graded meshes

We now recall the construction of special graded meshes for the finite element approximation of Eq. (5) introduced in [41]. Depending on the choice of the grading parameter, these meshes can yield finite element solutions with the optimal rate of convergence to singular solutions of (5).

Definition 3.7 (Graded Triangulations) Let \mathcal{T} be a triangulation of Ω whose vertices include S , such that no triangle in \mathcal{T} has more than one of its vertices in S . For

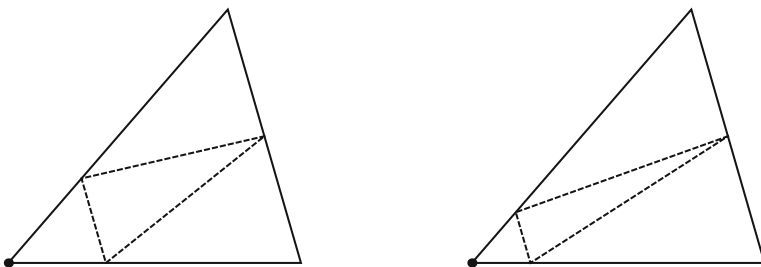


Fig. 2 A κ -refinement of a single triangle with singular point, denoted by filled circles; $\kappa = 1/3$ (left) and $\kappa = 1/5$ (right)

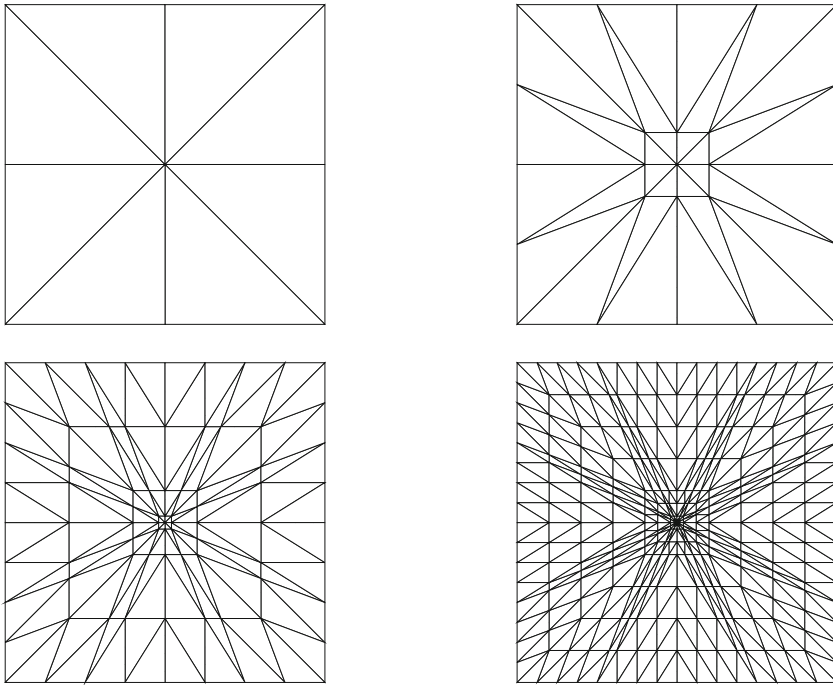


Fig. 3 Graded triangulations \mathcal{T}_0 – \mathcal{T}_3 , with $\kappa = 1/5$, grading toward the center point

$\kappa \in (0, 1/2]$, a κ refinement of \mathcal{T} , denoted by $\kappa(\mathcal{T})$, is obtained by dividing each edge AB of \mathcal{T} in two parts as follows:

- If neither A nor B is in S , then we divide AB into two equal parts.
- Otherwise, if say A is in S , we divide AB into AC and CB such that $|AC| = \kappa|AB|$.

This will divide each triangle of \mathcal{T} into four triangles (see Fig. 2). Given an initial triangulation \mathcal{T}_0 , the associated family of graded triangulations $\{\mathcal{T}_n : n \geq 0\}$ is defined recursively, $\mathcal{T}_{n+1} = \kappa(\mathcal{T}_n)$ (see Fig. 3). We see that $\dim(V_n) \sim 4^n$, because each refinement increases the number of triangles by precisely a factor of 4; and the same can be said for $\dim(W_n)$.

Remark 3.8 In practice it may be useful to have distinct grading parameters $\{\kappa_j : z_j \in S\}$ which are chosen based on a priori knowledge of the singular behavior of the weak solution u at these points. For example, at a convex corner $z \in S$ of Ω at which the boundary condition does not change type, one might naturally choose $\kappa_z = 1/2$ because the solution is locally at least in H^2 . The discussion in [41] indicates how the grading parameter(s) can be appropriately chosen more generally. For example, suppose $f \in \mathcal{K}_{a-1}^0$ for $0 < a < \min(\eta_z, 1)$ in a neighborhood of $z \in S$, where η_z is the local regularity index near z . In this case we choose the grading parameter $\kappa_z = 2^{-1/a}$ in the construction of the graded mesh near z .

The following convergence result is proven in [41, Theorem 4.12]:

Theorem 3.9 *Recall the regularity index η in Theorem 2.3. For any $0 < a < \hat{\eta} := \min(\eta, 1)$, choose $\kappa = 2^{-1/a}$. Then, on the resulting family of graded triangulations $\{\mathcal{T}_n\}$, in the manner of Definition 3.7 and Remark 3.8, the optimal order convergence is achieved for the solutions $u \in \mathcal{H}$ of (5) and $u_n \in V_n$ of (19):*

$$\|u - u_n\|_{\mathcal{K}_1^1(\Omega)} \leq C \dim(V_n)^{-1/2} \|f\|_{\mathcal{K}_{a-1}^0(\Omega)},$$

for a constant C which depends on the grading parameter(s), but not on f or n .

Remark 3.10 In [41], a more general result,

$$\|u - u_n\|_{\mathcal{K}_1^1(\Omega)} \leq C \dim(V_n)^{-m/2} \|f\|_{\mathcal{K}_{a-1}^{m-1}(\Omega)},$$

was proven, where V_n consists of the continuous functions in $\mathcal{K}_1^1(\Omega)$ which are in \mathbb{P}_m on each triangle, and the stronger grading parameter $\kappa = 2^{-m/a}$ is used for refinement. That result also allows for multiple grading parameters as in Remark 3.8.

4 Asymptotic exactness of the hierarchical error estimate

We carry out our a posteriori error analysis, using hierarchical-type error estimators, on appropriately graded meshes that satisfy the conditions of Theorem 3.9. The approximate error function, $\varepsilon_n \approx u - u_n$, will be proven to be asymptotically identical to $u - u_n$ in the energy-norm $\|\cdot\|$, thereby providing a useful criterion for determining when the error is below a certain tolerance. It will be convenient to use the following common notation: for quantities X, Y , we write $X \lesssim Y$ when $X \leq CY$ for some constant C which is independent of X and Y ; and we write $X \simeq Y$ when $X \lesssim Y$ and $Y \lesssim X$. In some of the arguments below, we abuse this notation slightly; for example, “ $X_1 \lesssim X_2 = X_3 \lesssim X_4 \leq X_5$ ” should be understood as “ $X_1 \lesssim X_2$ and $X_2 = X_3$ and $X_3 \lesssim X_4$ and $X_4 \leq X_5$ ”. This notational abuse more clearly indicates how the individual terms in the expression are related.

For convenience we let $N = \dim(V_n)$, and therefore $N \simeq 4^n$. Recall regularity index η in Theorem 2.3. We select a grading parameter $a < \hat{\eta} = \min(1, \eta)$, and $\kappa = 2^{-1/a}$. Let $\xi \in (a, \hat{\eta})$ be a constant with $\xi < 2a$. Throughout the results below, we assume that $u \in \mathcal{K}_{1+\xi}^3(\Omega)$, which will hold, for example, when $f \in \mathcal{K}_{\xi-1}^1(\Omega)$. The key result of this paper is

Theorem 4.1 *There is a $\sigma > 1/2$ for which $\|u - u_n - \varepsilon_n\| \lesssim N^{-\sigma} \|u\|_{\mathcal{K}_{1+\xi}^3(\Omega)}$. Therefore, if $\|u - u_n\| \simeq N^{-1/2}$, then*

$$\frac{\|\varepsilon_n\|}{\|u - u_n\|} \rightarrow 1 \quad \text{as } n \rightarrow \infty.$$

The bulk of this section is devoted to proving the first of these assertions, which is a consequence of (21) and Lemmas 4.5 and 4.12. The second assertion follows from

the first almost immediately. Since $\|u - u_n\| \simeq N^{-1/2}$, we have

$$\left| 1 - \frac{\|\varepsilon_n\|}{\|u - u_n\|} \right| = \frac{|\|u - u_n\| - \|\varepsilon_n\||}{\|u - u_n\|} \leq \frac{\|u - u_n - \varepsilon_n\|}{\|u - u_n\|} \lesssim N^{1/2-\sigma} \rightarrow 0.$$

An overview of the argument for the first assertion of Theorem 4.1 is as follows: Let $u_I = u_{I,n} \in V_n$ interpolate u at the vertices of the mesh \mathcal{T}_n , and $u_Q = u_{Q,n} \in V_n \oplus W_n$ interpolate u at the vertices and edge-midpoints of \mathcal{T}_n . It is clear that $u_B = u_{B,n} = u_Q - u_I \in W_n$. By definition, it holds that

$$\|u - u_n - \varepsilon_n\|^2 = B(u - u_n - \varepsilon_n, u - u_n - \varepsilon_n) = B(u - u_n - \varepsilon_n, u - u_n - u_B).$$

Therefore, $\|u - u_n - \varepsilon_n\| \leq \|u - u_n - u_B\|$. Using the triangle inequality and $u - u_n - u_B = (u - u_Q) + (u_I - u_n)$, we deduce that

$$\|u - u_n - \varepsilon_n\| \leq \|u - u_Q\| + \|u_I - u_n\|. \tag{21}$$

It remains to show that $\|u - u_Q\| = o(N^{-1/2})$ and $\|u_I - u_n\| = o(N^{-1/2})$. The first of these is perhaps not surprising (though it must be proved), but the assertion that $\|u_I - u_n\| = o(N^{-1/2})$ uses super-convergence properties which rely on the fact that most of the triangulation \mathcal{T}_n exhibits local mesh symmetries which can be carefully exploited to identify cancellations leading to higher-order convergence. Two common views of these local symmetries (or approximate symmetries) are represented in [14, 48]. The first of these focuses on points/vertices, considering patches of elements which are (approximately) symmetric with respect to the point. The second reference can be thought of as focussing on edges, considering pairs of triangles which form an (approximate) parallelogram. The superconvergence argument presented here builds on that of [19] for the Laplacian on graded meshes, which takes the view of [48] in terms of mesh symmetries. In our case, we must also address the term with the inverse-square potential.

Before moving on to the proof of Theorem 4.1, we briefly consider two related Hessian recovery results.

4.1 Hessian recovery in $W^{2,1}(\Omega)$

Although we generally expect that $u \notin H^2(\Omega)$, it is not unreasonable to expect that $u \in W^{2,1}(\Omega)$. This is certainly the case if u only has singularities of type r^α for $\alpha > 0$. In fact, we might reasonably expect that $u \in W^{2+s,1}(\Omega)$ for some $s \in (0, 1)$, and this does hold for the problems considered in Sect. 5. We present two lemmas concerning Hessian recovery in $W^{2,1}(\Omega)$, and revisit the result (22) in Sect. 5.

Lemma 4.2 *If $u \in W^{2,1}(\Omega)$ and $\sum_{T \in \mathcal{T}_n} |u - u_Q|_{W^{2,1}(T)} \rightarrow 0$ as $n \rightarrow \infty$, then*

$$\sum_{T \in \mathcal{T}_n} |\varepsilon_n|_{W^{2,1}(T)} \rightarrow |u|_{W^{2,1}(\Omega)} \text{ as } n \rightarrow \infty. \tag{22}$$

Proof We first prove that

$$\sum_{T \in \mathcal{T}_n} |\varepsilon_n - u_Q|_{W^{2,1}(T)} \rightarrow 0 \text{ as } n \rightarrow \infty.$$

The proof of Theorem 4.1 reveals that $\|\varepsilon_n - u_B\| \leq \|\|u - u_n - \varepsilon_n\| - \|u - u_n - u_B\|\| \lesssim N^{-\sigma}$ for some $\sigma > 1/2$. Therefore, $|\varepsilon_n - u_B|_{H^1(\Omega)} \lesssim N^{-\sigma}$ as well. We see that

$$\begin{aligned} \sum_{T \in \mathcal{T}_n} |\varepsilon_n - u_Q|_{W^{2,1}(T)} &= \sum_{T \in \mathcal{T}_n} |\varepsilon_n - u_B|_{W^{2,1}(T)} \lesssim \sum_{T \in \mathcal{T}_n} h_T^{-1} |\varepsilon_n - u_B|_{W^{1,1}(T)} \\ &\lesssim \sum_{T \in \mathcal{T}_n} |\varepsilon_n - u_B|_{H^1(T)} \leq \left(\sum_{T \in \mathcal{T}_n} 1 \right)^{1/2} |\varepsilon_n - u_B|_{H^1(\Omega)} \\ &\lesssim N^{1/2-\sigma} \rightarrow 0. \end{aligned}$$

We used equivalence of norms on finite dimensional spaces (three dimensional in this case) and a scaling argument to establish the inverse estimate $|\varepsilon_n - u_B|_{W^{2,1}(T)} \lesssim h_T^{-1} |\varepsilon_n - u_B|_{W^{1,1}(T)}$. Here, h_T is the diameter of T . Finally, since $|u - \varepsilon_n|_{W^{2,1}(T)} \leq |u - u_B|_{W^{2,1}(T)} + |\varepsilon_n - u_B|_{W^{2,1}(T)}$, if $\sum_{T \in \mathcal{T}_n} |u - u_Q|_{W^{2,1}(T)} \rightarrow 0$, then $\sum_{T \in \mathcal{T}_n} |u - \varepsilon_n|_{W^{2,1}(T)} \rightarrow 0$, which implies that $\sum_{T \in \mathcal{T}_n} |\varepsilon_n|_{W^{2,1}(T)} \rightarrow |u|_{W^{2,1}(\Omega)}$. This completes the proof. \square

The Lemma below provides a sufficient condition on u for which $\sum_{T \in \mathcal{T}_n} |\varepsilon_n|_{W^{2,1}(T)} \rightarrow |u|_{W^{2,1}(\Omega)}$.

Lemma 4.3 *Suppose that $u \in W^{2+s,1}(\Omega)$ for some $s \in (0, 1)$. Then*

$$\sum_{T \in \mathcal{T}_n} |u - u_Q|_{W^{2,1}(T)} \rightarrow 0 \text{ as } n \rightarrow \infty.$$

Proof Let \hat{T} be a reference element of diameter 1. For any function v on a triangle T , we define \hat{v} on \hat{T} in the usual way through affine transformation between \hat{T} and T . It holds that

$$|u - u_Q|_{W^{2,1}(T)} \lesssim |\hat{u} - \hat{u}_Q|_{W^{2,1}(\hat{T})} \leq |\hat{u} - \hat{P}|_{W^{2,1}(\hat{T})} + |\hat{P} - \hat{u}_Q|_{W^{2,1}(\hat{T})},$$

where the hidden constant is scale-invariant, and \hat{P} may be any quadratic polynomial on \hat{T} . Using the stability of quadratic Lagrange nodal interpolation (the Lagrange interpolant of \hat{P} is \hat{P}) together with a Sobolev imbedding result, we have

$$|\hat{P} - \hat{u}_Q|_{W^{2,1}(\hat{T})} \lesssim \|\hat{P} - \hat{u}\|_{L^\infty(\hat{T})} \lesssim \|\hat{P} - \hat{u}\|_{W^{2,1}(\hat{T})}.$$

At this stage, we choose \hat{P} to be the averaged Taylor polynomial of Dupont and Scott [24], and we see that

$$\begin{aligned} |u - u_Q|_{W^{2,1}(T)} &\lesssim \|\hat{u} - \hat{P}\|_{W^{2,1}(\hat{T})} \lesssim \|\hat{u} - \hat{P}\|_{W^{2+s,1}(\hat{T})} \lesssim |\hat{u}|_{W^{2+s,1}(\hat{T})} \\ &\lesssim h_T^s |u|_{W^{2+s,1}(T)}. \end{aligned}$$

The key inequality $\|\hat{u} - \hat{P}\|_{W^{2+s,1}(\hat{T})} \lesssim |\hat{u}|_{W^{2+s,1}(\hat{T})}$ is [24, Theorem 6.1], and the final inequality is merely a scaling argument.

Since the largest triangles in \mathcal{T}_n have diameter on the order of $2^{-n} \simeq N^{-1/2}$ (see Definition 4.4 below), it holds that

$$\sum_{T \in \mathcal{T}_n} |u - u_Q|_{W^{2,1}(T)} \lesssim \sum_{T \in \mathcal{T}_n} h_T^s |u|_{W^{2+s,1}(T)} \leq N^{-s/2} |u|_{W^{2+s,1}(\Omega)}.$$

This completes the proof. \square

4.2 The proof of Theorem 4.1

We specify the following geometric properties of our graded meshes to carry out further analysis.

Definition 4.4 (*Mesh layers*) Recall that the triangulation \mathcal{T}_j , $0 \leq j \leq n$, is obtained after j successive graded refinements of \mathcal{T}_0 with parameter κ (see Definition 3.7 and Remark 2.4). Let $\mathbb{T}_j \subset \mathcal{T}_j$ be the union of (closed) triangles in \mathcal{T}_j having a point in S as a vertex. Namely, \mathbb{T}_j is the immediate neighborhood of S in \mathcal{T}_j . Then, the j th layer of the mesh \mathcal{T}_n is defined as

$$L_0 = \Omega \setminus \mathbb{T}_1, \quad L_j = \mathbb{T}_{j-1} \setminus \mathbb{T}_j, \quad 1 \leq j < n, \quad L_n = \mathbb{T}_n.$$

It is apparent that $\Omega = \mathbb{T}_n \cup (\cup_j L_j)$. Based on Definition 3.7, the characteristic diameter of the triangles in L_j is $h_j \simeq \kappa^j 2^{j-n}$ for $j \leq n$, and $\vartheta \simeq \kappa_j$ on L_j for $j < n$. On L_n , $\vartheta \lesssim \kappa^n$.

We provide the following guide through the technical arguments below. As indicated in (21), the two key results to prove are that $\|u - u_Q\|$ and $\|u_I - u_n\|$ converge to zero more rapidly than $\|u - u_n\|$. The first of these, Lemma 4.5, follows readily enough from a few results proven elsewhere; but the second, Lemma 4.12, requires more delicate estimation, and we break up its analysis into a sequence of intermediate lemmas whose goal is to provide sufficiently sharp bounds on the pointwise error vector \mathbf{e} and the residual vector \mathbf{r} for which $\|u_I - u_n\|^2 = \mathbf{r}^t \mathbf{e}$ (see (25) and (26)). The bounds for \mathbf{e} and \mathbf{r} , namely Lemmas 4.9 and 4.10, are themselves established through a series of intermediate technical results. For the analysis of \mathbf{e} , it is useful to move between functional and linear algebraic perspectives when considering the weighted L^2 -norm of $u_I - u_n$, hence the consideration of the associated mass matrix M in Lemma 4.8. The estimates for \mathbf{r} requires certain mesh symmetries in the bulk of the domain, and

the analysis naturally splits into three categories: portions of the domain adjacent to singular points (33), and portions of the domain away from singular points where meshes symmetries are present (36) or are not present (37). The second key lemma, Lemma 4.12, follows from the careful accounting of the different contributions to the error bound that was done in Lemmas 4.9 and 4.10.

Lemma 4.5 *It holds that $\|u - u_Q\| \lesssim N^{-\xi/(2a)} \|u\|_{\mathcal{K}_{\xi+1}^3(\Omega)}$.*

Proof In [41, Lemma 4.8] it is shown that, in the final layer L_n (adjacent to singular points),

$$\|u - u_Q\|_{L_n} \lesssim \kappa^{n\xi} \|u\|_{\mathcal{K}_{1+\xi}^3(L_n)} \lesssim 2^{-n\xi/a} \|u\|_{\mathcal{K}_{1+\xi}^3(L_n)}. \tag{23}$$

For other layers $L_j, 0 \leq j < n$, it holds that (cf. [41, Lemma 4.4])

$$\begin{aligned} \|u - u_Q\|_{L_j} &\lesssim \kappa^{ja} \left(\frac{h_j}{\kappa^j}\right)^2 \|u\|_{\mathcal{K}_{1+a}^3(L_j)} \lesssim 2^{j-2n} \|u\|_{\mathcal{K}_{1+a}^3(L_j)} \\ &\lesssim 2^{j-2n} \kappa^{j(\xi-a)} \|u\|_{\mathcal{K}_{1+\xi}^3(L_j)} = 2^{-2n+(2-\xi/a)j} \|u\|_{\mathcal{K}_{1+\xi}^3(L_j)}. \end{aligned}$$

The inequality $\|u\|_{\mathcal{K}_{1+a}^3(L_j)} \lesssim \kappa^{j(\xi-a)} \|u\|_{\mathcal{K}_{1+\xi}^3(L_j)}$ follows from [41, Lemma 2.6(b)]. The assumption that $\xi < 2a$ ensures that $2 - \xi/a > 0$, so that $2^{-2n+(2-\xi/a)j}$ is maximized when $j = n$. Therefore,

$$\|u - u_Q\|_{L_j} \lesssim 2^{-2n+(2-\xi/a)n} \|u\|_{\mathcal{K}_{1+\xi}^3(L_j)} = 2^{-n\xi/a} \|u\|_{\mathcal{K}_{1+\xi}^3(L_j)}. \tag{24}$$

Combining (23) and (24) completes the proof. □

Let $\phi_i \in V_n$ denote the piecewise-linear basis function satisfying $\phi_i(z_j) = \delta_{ij}$ for each vertex z_j in the mesh \mathcal{T}_n , and let ω_i denote its support. Therefore, ω_i is the patch of triangles having z_i as a vertex. It holds that

$$\|u_I - u_n\|^2 = B(u_n - u_I, u_n - u_I) = B(u - u_I, u_n - u_I) = \mathbf{r}^t \mathbf{e} \leq \|\mathbf{r}\| \|\mathbf{e}\|, \tag{25}$$

where $\mathbf{r}, \mathbf{e} \in \mathbb{R}^N$ are given by

$$\mathbf{r}_i = B(u - u_I, \phi_i), \quad \mathbf{e}_i = (u_n - u_I)(z_i) \tag{26}$$

and $\|\cdot\|$ is the Euclidean norm.

We begin by analyzing $\|\mathbf{e}\|$, and do so by first introducing the weighted L^2 inner-product,

$$(v, w)_{p_2} = (Pv, Pw) \quad \text{where } P|_{L_j} = (2\kappa)^{-j}. \tag{27}$$

We use $\|\cdot\|_{p_2}$ to denote the induced norm. The weighted L^2 mass matrix $M \in \mathbb{R}^{N \times N}$, given by

$$m_{i,j} = (\phi_i, \phi_j)_{p_2},$$

will also play a role in the analysis.

Lemma 4.6 *It holds that $\|u - u_I\|_{\mathcal{K}_1^0(L_n)} \lesssim \kappa^{n\xi} \|u\|_{\mathcal{K}_{\xi+1}^2(L_n)}$.*

Proof For a singular point $y \in S$, it is clear that with several graded refinements, the function $\vartheta|_{L_n}$ equals the distance to y . Using a simple translation if necessary, we see that we lose no generality by assuming that $y = 0$. Let $\widehat{L}_n := \lambda^{-1}L_n$, where $\lambda = \kappa^n$. Then, we define the dilation of a function on \widehat{L}_n ,

$$v_\lambda(x) = v(\lambda x), \quad \forall x \in \widehat{L}_n.$$

Then, by Lemma 4.3 in [41],

$$\|v_\lambda\|_{\mathcal{K}_\mu^m(\widehat{L}_n)} = \lambda^{\mu-1} \|v\|_{\mathcal{K}_\mu^m(L_n)}. \tag{28}$$

Let χ be a smooth function that equals 0 in a neighborhood of y and equals 1 at all the nodal points of \widehat{L}_n . Then, since $\chi u = 0$ in the neighborhood of y , we first have for $0 \leq m \leq 2$,

$$\|(\chi u)_\lambda\|_{H^m(\widehat{L}_n)} \lesssim \|(\chi u)_\lambda\|_{\mathcal{K}_1^m(\widehat{L}_n)} \lesssim \|(\chi u)_\lambda\|_{H^m(\widehat{L}_n)}, \tag{29}$$

$$\|(\chi u)_\lambda\|_{\mathcal{K}_1^m(\widehat{L}_n)} \lesssim \|u_\lambda\|_{\mathcal{K}_1^m(\widehat{L}_n)}. \tag{30}$$

Note that u_I is also the interpolant of χu on L_n by the definition. Therefore, by (28), (29), (30), and the definition of the weighted spaces, we have

$$\begin{aligned} \|u - u_I\|_{\mathcal{K}_1^0(L_n)} &\leq \|u - \chi u\|_{\mathcal{K}_1^0(L_n)} + \|\chi u - u_I\|_{\mathcal{K}_1^0(L_n)} \\ &= \|u_\lambda - (\chi u)_\lambda\|_{\mathcal{K}_1^0(\widehat{L}_n)} + \|(\chi u)_\lambda - u_{\lambda I}\|_{\mathcal{K}_1^0(\widehat{L}_n)} \\ &\lesssim (\|u_\lambda\|_{\mathcal{K}_1^0(\widehat{L}_n)} + \|(\chi u)_\lambda\|_{H^2(\widehat{L}_n)}) \\ &\lesssim \|u_\lambda\|_{\mathcal{K}_1^2(\widehat{L}_n)} = \|u\|_{\mathcal{K}_1^2(L_n)} \lesssim \kappa^{n\xi} \|u\|_{\mathcal{K}_{\xi+1}^2(L_n)}. \end{aligned}$$

This completes the proof. □

Lemma 4.7 *It holds that $\|u_I - u_n\|_{p_2} \lesssim N^{-1} \|u\|_{\mathcal{K}_{\xi+1}^2(\Omega)}$.*

Proof The proof is based on estimates for $\|u - u_I\|_{p_2}$ and $\|u - u_n\|_{p_2}$. To show that $\|u - u_n\|_{p_2} \lesssim N^{-1} \|u\|_{\mathcal{K}_{\xi+1}^2(\Omega)}$, we begin with a standard duality-type argument. Let $w \in \mathcal{H}$ be the unique function satisfying $B(w, v) = (P^2(u - u_n), v)$ for all $v \in \mathcal{H}$. Choosing $v = u - u_n$, we have

$$\begin{aligned} \|u - u_n\|_{p_2}^2 &= B(w, u - u_n) = B(w - w_n, u - u_n) \lesssim \|w - w_n\|_{\mathcal{K}_1^1(\Omega)} \|u - u_n\|_{\mathcal{K}_1^1(\Omega)} \\ &\lesssim N^{-1/2} \|P^2(u - u_n)\|_{\mathcal{K}_{a-1}^0(\Omega)} N^{-1/2} \|u\|_{\mathcal{K}_{a+1}^2(\Omega)}. \end{aligned}$$

Note that

$$\begin{aligned} \|P^2(u - u_n)\|_{\mathcal{K}_{a-1}^0(\Omega)}^2 &= \sum_{j \leq n} \|P^2 \vartheta^{1-a}(u - u_n)\|_{L^2(L_j)}^2 \\ &\lesssim \sum_{j \leq n} \|P(2\kappa)^{-j}(\kappa^j)^{1-a}(u - u_n)\|_{L^2(L_j)}^2 \\ &= \sum_{j \leq n} \|P(u - u_n)\|_{L^2(L_j)}^2 = \|u - u_n\|_{P^2}^2. \end{aligned}$$

Here we used $(2\kappa)^{-j}(\kappa^j)^{1-a} = 2^{-j}\kappa^{-ja} = 1$. Therefore, we have established

$$\|u - u_n\|_{P^2} \lesssim N^{-1} \|u\|_{\mathcal{K}_{a+1}^2(\Omega)} \lesssim N^{-1} \|u\|_{\mathcal{K}_{\xi+1}^2(\Omega)}. \tag{31}$$

We now turn to $\|u - u_I\|_{P^2}$, beginning with the identity

$$\|u - u_I\|_{P^2}^2 = \sum_{j \leq n} (2\kappa)^{-2j} \|u - u_I\|_{L^2(L_j)}^2.$$

For $j < n$, we have

$$\begin{aligned} (2\kappa)^{-2j} \|u - u_I\|_{L^2(L_j)}^2 &= (2\kappa)^{-2j} \sum_{T \subset L_j} \|u - u_I\|_{L^2(T)}^2 \lesssim (2\kappa)^{-2j} h_j^4 |u|_{H^2(L_j)}^2 \\ &= (2\kappa)^{-2j} h_j^4 \kappa^{-2j(1-\xi)} |\kappa^{j(1-\xi)} u|_{H^2(L_j)}^2 \\ &\lesssim (2\kappa)^{-2j} h_j^4 \kappa^{-2j(1-\xi)} |u|_{\mathcal{K}_{1+\xi}^2(L_j)}^2 \\ &= 2^{-4n-2(\xi/a-1)j} |u|_{\mathcal{K}_{1+\xi}^2(L_j)}^2 \leq 2^{-4n} |u|_{\mathcal{K}_{1+\xi}^2(L_j)}^2. \end{aligned}$$

Using Lemma 4.6 on L_n , we have

$$\begin{aligned} \|(2\kappa)^{-n}(u - u_I)\|_{L^2(L_n)}^2 &\lesssim 2^{-2n} \|u - u_I\|_{\mathcal{K}_1^0(L_n)}^2 \lesssim 2^{-2n} \kappa^{2n\xi} \|u\|_{\mathcal{K}_{\xi+1}^2(L_n)}^2 \\ &= 2^{-2n-2n\xi/a} \|u\|_{\mathcal{K}_{\xi+1}^2(L_n)}^2 \leq 2^{-4n} \|u\|_{\mathcal{K}_{\xi+1}^2(L_n)}^2. \end{aligned}$$

Finally, summing over layers, we obtain

$$\|u - u_I\|_{P^2}^2 = \sum_{j \leq n} (2\kappa)^{-2j} \|u - u_I\|_{L^2(L_j)}^2 \lesssim 2^{-4n} |u|_{\mathcal{K}_{1+\xi}^2(\Omega)}^2 \lesssim N^{-2} |u|_{\mathcal{K}_{1+\xi}^2(\Omega)}^2. \tag{32}$$

The proof is completed by combining (31) and (32). □

Lemma 4.8 *The matrix M is symmetric and positive definite, and $\mathbf{v}^t M \mathbf{v} \simeq N^{-1} \mathbf{v}^t \mathbf{v}$ for any $\mathbf{v} \in \mathbb{R}^N$, where the constants of equivalence depend only on κ .*

Proof Since M is a Gram matrix (arising from an inner-product), and $\{\phi_i : 1 \leq i \leq N\}$ is a linearly independent set, M is symmetric and positive definite. We identify $v \in V_n$ with its coefficient vector $\mathbf{v} \in \mathbb{R}^N$. It holds that

$$\mathbf{v}^t M \mathbf{v} = \|Pv\|_{0,\Omega}^2 = \sum_{j=0}^n \sum_{T \subset L_j} \|Pv\|_{0,T}^2 = \sum_{j=0}^n \sum_{T \subset L_j} (2\kappa)^{-2j} \|v\|_{0,T}^2.$$

Taking \mathbf{v}_T to consist of the components of \mathbf{v} which are associated with the non-Dirichlet vertices of T , we estimate $\|v\|_{0,T}^2$ in terms of $\|\mathbf{v}_T\|^2$. We lose no generality by assuming that all three vertices of T correspond to degrees of freedom, therefore $\mathbf{v}_T \in \mathbb{R}^3$. It holds that

$$\|v\|_{0,T}^2 = \mathbf{v}_T^t R_T \mathbf{v}_T \quad \text{where} \quad R_T = |T| \begin{pmatrix} 2 & 1 & 1 \\ 1 & 2 & 1 \\ 1 & 1 & 2 \end{pmatrix},$$

and $\lambda_{\max}(R_T) = 4|T|, \lambda_{\min}(R_T) = |T|$. Since $|T| \simeq h_j^2 \simeq (2^{j-n}\kappa^j)^2$ for each $T \in L_j$, we deduce that

$$\begin{aligned} \mathbf{v}^t M \mathbf{v} &\simeq \sum_{j \leq n} \sum_{T \subset L_j} (2\kappa)^{-2j} (2^{j-n}\kappa^j)^2 \mathbf{v}_T^t \mathbf{v}_T = \sum_{j \leq n} \sum_{T \subset L_j} N^{-1} \mathbf{v}_T^t \mathbf{v}_T \\ &= N^{-1} \sum_{T \in \mathcal{T}_n} \mathbf{v}_T^t \mathbf{v}_T \simeq N^{-1} \mathbf{v}^t \mathbf{v}. \end{aligned}$$

This completes the argument. □

Lemmas 4.7 and 4.8 combine to give a bound on $\|\mathbf{e}\|$.

Lemma 4.9 *It holds that $\|\mathbf{e}\| \lesssim N^{-1/2} \|u\|_{\mathcal{K}_{\xi+1}^2(\Omega)}$, where the hidden constant depends only on ξ and the grading parameter a .*

Proof We see that

$$\|\mathbf{e}\|^2 \simeq N \mathbf{e}^t M \mathbf{e} = N \|u_I - u_n\|_{p^2}^2 \lesssim N^{-1} \|u\|_{\mathcal{K}_{\xi+1}^2(\Omega)}^2,$$

which completes the argument. □

We now consider the quantities $\mathbf{r}_i = B(u - u_I, \phi_i)$ for various scenarios, beginning with the case $\omega_i \cap L_n \neq \emptyset$. It holds that

$$|\mathbf{r}_i| = |B(u - u_I, \phi_i)| \leq \|u - u_I\| \|\phi_i\| \lesssim \kappa^{n\xi} \|u\|_{\mathcal{K}_{\xi+1}^2(\omega_i)} \|\phi_i\| \lesssim 2^{-n\xi/a} \|u\|_{\mathcal{K}_{\xi+1}^2(\omega_i)}. \tag{33}$$

The result $\|u - u_I\| \leq C \kappa^{n\xi} \|u\|_{\mathcal{K}_{\xi+1}^2(\omega_i)}$ is established in [41]. Lemma 3.1 guarantees that $|\phi|_{1,\omega_i}$ is bounded by a constant depending only on the shape regularity of ω_i ,

which is governed purely by the grading ratio κ , and the argument used in the proof of Lemma 3.2 can be used here to establish that this is also the case for $\|r^{-1}\phi_i\|_{0,\omega_i}$. Therefore, $\|\phi_i\| \leq C$.

For patches ω_i intersecting layer L_j , $0 \leq j < n$, we distinguish two categories: those which are symmetric about z_i , and those which are not. A patch ω_i is said to be symmetric about z_i if $z_i - (x - z_i) \in \omega_i$ whenever $x \in \omega_i$. For a symmetric patch $\omega_i \subset L_j$, it is proven in [20] that $|(\nabla(u - u_I), \nabla\phi_i)| \lesssim h_j^2|u|_{3,\omega_i}$; for a fuller discussion of the relationship between local mesh symmetries and super-convergence properties, see [48]. From this we deduce that

$$\begin{aligned} |(\nabla(u - u_I), \nabla\phi_i)| &\lesssim h_j^2(\kappa^j)^{\xi-2}|u|_{\mathcal{K}_{\xi+1}^3(\omega_i)} \lesssim \kappa^{j\xi}2^{2(j-n)}|u|_{\mathcal{K}_{\xi+1}^3(\omega_i)} \\ &= 2^{-2n+(2-\xi/a)j}|u|_{\mathcal{K}_{\xi+1}^3(\omega_i)} \lesssim 2^{-n\xi/a}|u|_{\mathcal{K}_{\xi+1}^3(\omega_i)}. \end{aligned} \tag{34}$$

For a general patch $\omega_i \subset L_j$, $0 \leq j < n$, it also holds that

$$\begin{aligned} |(r^{-2}(u - u_I), \phi_i)| &\lesssim \kappa^{-2j}\|u - u_I\|_{0,\omega_i}\|\phi_i\|_{0,\omega_i} \lesssim \kappa^{-2j}h_j^2|u|_{2,\omega_i}h_j \\ &\lesssim \kappa^{-2j}h_j^3(\kappa^j)^{\xi-1}|u|_{\mathcal{K}_{\xi+1}^2(\omega_i)} \lesssim 2^{-3n+(3-\xi/a)j}|u|_{\mathcal{K}_{\xi+1}^2(\omega_i)} \\ &\lesssim 2^{-n\xi/a}|u|_{\mathcal{K}_{\xi+1}^2(\omega_i)}. \end{aligned} \tag{35}$$

Combining these results in (34) and (35), we see that, for a symmetric patch ω_i in layer L_j , $j < n$,

$$|\mathbf{r}_i| = |B(u - u_I, \phi_i)| \lesssim 2^{-n\xi/a}\|u\|_{\mathcal{K}_{\xi+1}^3(\omega_i)}. \tag{36}$$

We now consider non-symmetric patches ω_i which intersect layer L_j , $0 \leq j < n$, but do not intersect L_n . For any $0 < s < 1$, it holds that

$$\begin{aligned} |(\nabla(u - u_I), \nabla\phi_i)| &\leq \|\nabla(u - u_I)\|_{L^\infty(\omega_i)}\|\nabla\phi_i\|_{L^1(\omega_i)} \lesssim h_j^s\|u\|_{W_\infty^{1+s}(\omega_i)}|\omega_i|^{1/2} \\ &\lesssim h_j^s\kappa^{j(\xi-2)}\|\kappa^{j(2-\xi)}u\|_{W_\infty^{1+s}(\omega_i)}|\omega_i|^{1/2} \\ &\lesssim h_j^s\kappa^{j(\xi-2)}\|\vartheta^{2-\xi}u\|_{W_\infty^{1+s}(\omega_i)}|\omega_i|^{1/2}. \end{aligned}$$

The analysis of $|(r^{-2}(u - u_I), \phi_i)|$ is the same as for the symmetric case. Combining the above, we see that for non-symmetric patches ω_i intersecting L_j but not L_n ,

$$|\mathbf{r}_i|^2 = |B(u - u_I, \phi_i)|^2 \lesssim \kappa^{2j(\xi-2)}h_j^{2s}\|\vartheta^{2-\xi}u\|_{W_\infty^{1+s}(\omega_i)}^2|\omega_i| + 2^{-2n\xi/a}|u|_{\mathcal{K}_{\xi+1}^2(\omega_i)}^2. \tag{37}$$

Lemma 4.10 *Let $\xi \in (a, \hat{\eta})$ with $\xi \leq 3a/2$. There is a $\sigma > 1/2$ for which $\|\mathbf{r}\| \lesssim N^{-\sigma}\|u\|_{\mathcal{K}_{\xi+1}^3(\Omega)}$.*

Proof Let $I_n = \{i : \omega_i \cap L_n \neq \emptyset\}$. It follows from (33) that

$$\begin{aligned} \sum_{i \in I_n} |\mathbf{r}_i|^2 &\lesssim 2^{-2n\xi/a} \sum_{i \in I_n} \|u\|_{\mathcal{K}_{\xi+1}^3(\omega_i)}^2 \\ &\lesssim 2^{-2n\xi/a} \|u\|_{\mathcal{K}_{\xi+1}^3(L_n \cup L_{n-1})}^2 \leq 2^{-2n\xi/a} \|u\|_{\mathcal{K}_{\xi+1}^3(\Omega)}^2. \end{aligned}$$

Let $I_j = \{i : \omega_i \subset L_j \text{ and } \omega_i \text{ is symmetric}\}$, for $j < n$. It follows from (36) that

$$\begin{aligned} \sum_{j < n} \sum_{i \in I_j} |\mathbf{r}_i|^2 &\lesssim \sum_{j < n} \sum_{i \in I_j} 2^{-2n\xi/a} \|u\|_{\mathcal{K}_{\xi+1}^3(\omega_i)}^2 \lesssim 2^{-2n\xi/a} \sum_{j < n} \|u\|_{\mathcal{K}_{\xi+1}^3(L_j)}^2 \\ &\leq 2^{-2n\xi/a} \|u\|_{\mathcal{K}_{\xi+1}^3(\Omega)}^2 \end{aligned}$$

The analysis for non-symmetric patches is a little more involved. Let

$$J_j = \{i : \omega_i \cap L_j \neq \emptyset, \omega_i \cap L_n = \emptyset \text{ and } \omega_i \text{ is not symmetric}\},$$

for $j < n$. It is shown in [19] that

$$\sum_{i \in J_j} |\omega_i| \lesssim \kappa^j h_j. \tag{38}$$

Using (37), we see that

$$\begin{aligned} \sum_{j < n} \sum_{i \in J_j} |\mathbf{r}_i|^2 &\lesssim \sum_{j < n} \sum_{i \in J_j} 2^{-2n\xi/a} |u|_{\mathcal{K}_{\xi+1}^2(\omega_i)}^2 + \sum_{j < n} \sum_{i \in J_j} \kappa^{2j(\xi-2)} h_j^{2s} \|\vartheta^{2-\xi} u\|_{W_\infty^{1+s}(\omega_i)}^2 |\omega_i| \\ &\lesssim 2^{-2n\xi/a} \|u\|_{\mathcal{K}_{\xi+1}^2(\Omega)}^2 + \|\vartheta^{2-\xi} u\|_{W_\infty^{1+s}(\Omega \setminus L_n)}^2 \sum_{j < n} \kappa^{2j(\xi-2)} h_j^{2s} \kappa^j h_j. \end{aligned}$$

For the second inequality, we used (38) to bound the latter sum. By the definitions of the corresponding spaces and the Sobolev imbedding theorem for $0 < s < 1$, we have

$$\|\vartheta^{2-\xi} u\|_{W_\infty^{1+s}(\Omega \setminus L_n)} \leq \|\vartheta^{2-\xi} u\|_{W_\infty^{1+s}(\Omega)} \lesssim \|\vartheta^{2-\xi} u\|_{H^3(\Omega)} \lesssim \|u\|_{\mathcal{K}_{\xi+1}^3(\Omega)}.$$

From this, we obtain

$$\sum_{j < n} \sum_{i \in J_j} |\mathbf{r}_i|^2 \lesssim \left(2^{-2n\xi/a} + \sum_{j < n} \kappa^{2j(\xi-2)} h_j^{2s} \kappa^j h_j \right) \|u\|_{\mathcal{K}_{\xi+1}^3(\Omega)}^2.$$

For any $\rho \in (0, 1)$, with $s = 1 - \rho$, we have

$$\begin{aligned} \kappa^{2j(\xi-2)} h_j^{2s} \kappa^j h_j &= \kappa^{j(2\xi-3)} h_j^{2s+1} \lesssim \kappa^{j(2\xi-3)} \kappa^{j(2s+1)} 2^{(j-n)(2s+1)} \\ &= \kappa^{2j(s+\xi-1)} 2^{(j-n)(2s+1)} \\ &= \kappa^{2j(\xi-\rho)} 2^{(j-n)(3-2\rho)} = 2^{j[(3a-2\xi)+2\rho(\xi-\rho)]/a} 2^{-n(3-2\rho)}. \end{aligned}$$

As a temporary notational convenience, let $\phi = [(3a - 2\xi) + 2\rho(\xi - \rho)]/a$. We lose no generality by assuming that $\xi > \rho$, therefore $\phi > 0$. We have

$$\sum_{j < n} \kappa^{2j(\xi-2)} h_j^{2s} \kappa^j h_j = 2^{-n(3-2\rho)} \frac{2^{n\phi} - 1}{2^\phi - 1} \leq \frac{2^{-2n(\xi/a-\rho(\xi+a-\rho)/a)}}{2^{3-2\xi/a} - 1}.$$

At this stage we see that, for any $\epsilon > 0$, we may choose $\rho > 0$ small enough so that

$$\sum_{j < n} \sum_{i \in J_j} |\mathbf{r}_i|^2 \lesssim 2^{-2n(\xi/a-\epsilon)} \|u\|_{\mathcal{K}_{\xi+1}^3(\Omega)}^2 \lesssim N^{-(\xi/a-\epsilon)} \|u\|_{\mathcal{K}_{\xi+1}^3(\Omega)}^2.$$

Combining this result with those for L_n and the symmetric patches in L_j for $j < n$, we finally obtain

$$\|\mathbf{r}\|^2 \lesssim N^{-(\xi/a-\epsilon)} \|u\|_{\mathcal{K}_{\xi+1}^3(\Omega)}^2,$$

from which the assertion of the lemma follows directly. □

Remark 4.11 A similar argument to that given in Lemma 4.10 could be made for $3a/2 < \xi < \min(2a, \hat{\eta})$, again showing that $\|\mathbf{r}\| = o(N^{-1/2})$. In light of this, the restriction $\xi \leq 3a/2$, though convenient for the proof, is not necessary, and one can replace this with the assumption $\xi < 2a$ used in prior lemmas.

Lemmas 4.9 and 4.10 combine to yield the superconvergence result below, the last essential component in the proof of Theorem 4.1.

Lemma 4.12 *There is a $\sigma > 1/2$ for which $\|u_I - u_n\| \lesssim N^{-\sigma} \|u\|_{\mathcal{K}_{\xi+1}^3(\Omega)}$.*

5 Numerical experiments

We provide numerical experiments solving Eq. (5) on three different domains using the corresponding optimally graded meshes described in Theorem 3.9. These problems represent three typical scenarios for the model problem: (1) an interior singularity resulting from the singular potential (Sect. 5.1), (2) a boundary singularity resulting from a combination of a singular potential and a re-entrant (non-convex) corner at which a switch in the boundary conditions takes place (Sect. 5.2), and (3) multiple singularities from the singular potential and the non-smoothness of the domain, respectively (Sect. 5.3). In these experiments, u_n denotes the discrete solution on the

triangulation \mathcal{T}_n , which has $N = N(n)$ triangles. For the graded (a priori) refinement, $N(n + 1) = 4N(n)$. As an interesting comparison, we also test these problems on adaptive (a posteriori) meshes. Note that the underlying mechanism for the adaptive (a posteriori) approximation is quite different from the graded (a priori) approximation. The theoretical justification of these adaptive approximations shall be studied in the future work. In the adaptive refinement simulations, we still use u_n to denote the discrete solution.

In addition to the convergence rate of the numerical solution, we report the effectivity $\|\varepsilon_n\|/\|u - u_n\|$ for both the energy norm $\|\cdot\|$ and the H^1 -seminorm $|\cdot|_1$, noting the observed asymptotic exactness. These (exact) convergence rates and effectivities are provided in Sects. 5.1 and 5.2, where the exact solutions are known. In Sect. 5.3, we use $\|\varepsilon_n\|$ as a proxy for the actual error $\|u - u_n\|$ in our convergence plots, and do not estimate the effectivities. In all graphs, $N = N(n)$ is given on the horizontal axis, and the quantity of interest (error, effectivity, condition number) on the vertical axis. As such, axes are not given labels, and the quantities of interest are described in the accompanying captions.

The software package PLTMG [9] was used for these experiments, with suitable modifications for employing hierarchical error estimation and graded mesh refinement. We note a few details concerning the adaptive refinement algorithm, which is more sophisticated than many of the commonly-used approaches in similar software. All current elements are placed in a heap data structure according to the size of the local error indicators. Here, we use estimates of local H^1 -semi-norm error, $|\varepsilon_n|_{1,T}$, to drive the adaptive refinement even if we are concerned with error in the energy norm. The element with largest error estimate is at the root of the heap, and is selected for refinement. The longest-edge bisection of Rivara [47] is used to refine this triangle and a minimal number of neighbors in order to produce a valid triangulation (no hanging nodes). Error indicators are immediately computed for each of the new elements, and the heap is updated, with the new “worst” triangle marked for refinement. This continues until the total number of elements has been increased by roughly a factor of four, which is the rate of increase in elements for the graded refinement approach. This refinement approach allows for a more aggressive refinement toward detected singularities. The refined mesh is then post-processed to improve the quality of triangles (shape-regularity)—i.e. make them closer to being equilateral. This is done by a combination of edge-swapping and mesh smoothing [12], in such a way as to preserve the locations of specific “flagged” points, such as those in the singular set S . We briefly return to the issue of computing local error indicators on new elements without resolving (19)–(20) on the intermediate meshes. Any function in W_n , when restricted to a triangle, is uniquely determined by the geometry of that triangle and its Hessian on the triangle. Because of this, error indicators may be immediately obtained for the children of a triangle by adopting the Hessian of the parent. Of course, the quality of these indicators will deteriorate if too many refinements are done before a new problem is solved, but extensive empirical evidence suggests that this approach is very effective. Because the Hessian of ε_n is used (locally) in the adaptive scheme, we provide numerical evidence below that it, in some sense, approximates the Hessian of u .

Table 1 Errors and effectivities for the unit disk, $\delta = 0.5$: adaptive refinement driven by local indicators (top); graded refinement with $\kappa = 0.375$ (middle); graded refinement with $\kappa = 0.2$ (bottom)

N	$\ u - u_n\ $	EFF	$ u - u_n _1$	EFF
8	1.4677E+00	1.4186	1.2119E+00	1.4729
94	4.5930E-01	1.0076	4.1764E-01	1.0598
452	2.1335E-01	0.8932	1.9068E-01	0.9842
1,921	9.7086E-02	0.9717	9.4121E-02	0.9928
7,865	4.5802E-02	0.9808	4.5172E-02	0.9908
31,783	2.1953E-02	0.9881	2.1846E-02	0.9917
127,740	1.0755E-02	0.9915	1.0738E-02	0.9926
8	1.4677E+00	1.4186	1.2119E+00	1.4729
32	8.0950E-01	1.0877	7.7101E-01	1.0895
128	4.1937E-01	1.0207	4.0920E-01	1.0279
512	2.1579E-01	1.0013	2.1121E-01	1.0136
2,048	1.1109E-01	0.9949	1.0901E-01	1.0070
8,192	5.7162E-02	0.9926	5.6142E-02	1.0046
32,768	2.9380E-02	0.9923	2.8895E-02	1.0034
131,072	1.5081E-02	0.9922	1.4842E-02	1.0030
8	1.4677E+00	1.4186	1.2119E+00	1.4729
32	9.9004E-01	1.0702	9.5710E-01	1.0485
128	5.0505E-01	1.0217	4.9974E-01	1.0159
512	2.5477E-01	1.0064	2.5391E-01	1.0051
2,048	1.2808E-01	1.0023	1.2797E-01	1.0019
8,192	6.4267E-02	1.0005	6.4247E-02	1.0004
32,768	3.2192E-02	1.0002	3.2188E-02	1.0002
131,072	1.6121E-02	0.9993	1.6112E-02	0.9998

5.1 The unit disk with the singularity at the center

For this example, we consider the unit disk $\Omega = \{(x, y) : x^2 + y^2 < 1\}$, with homogeneous Dirichlet boundary conditions. If $f = 4 - \delta$ in (2), then the exact solution is given by $u = r^{\sqrt{\delta}} - r^2$. We recall that optimal order of convergence for graded meshes will be achieved for grading parameters $0 < \kappa < 2^{-1/a}$ for $0 < a < \eta = \sqrt{\delta}$. We investigate the cases $\delta = 0.5, 0.25, 0.0625$, with the most detail given for $\delta = 0.5$.

In the case $\delta = 0.5$, errors and effectivities are reported in Table 1 for both graded refinement and adaptive refinement as described above. We consider both $\kappa = 0.375 \approx 2^{-\sqrt{2}}$ and the more aggressive grading $\kappa = 0.2$. In each case, the errors decrease at the optimal rate $\dim(V_n)^{-1/2} \sim N^{-1/2}$ in both norms, and the effectivities remain near 1 throughout the refinement process. We see that the adaptive refinement yields the smallest errors for comparable problem sizes; with the less aggressive grading, $\kappa = 0.375$, faring a little better than $\kappa = 0.2$. Figure 4 contains triangulations generated by each of the refinement approaches. As a matter of interest, we briefly indicate

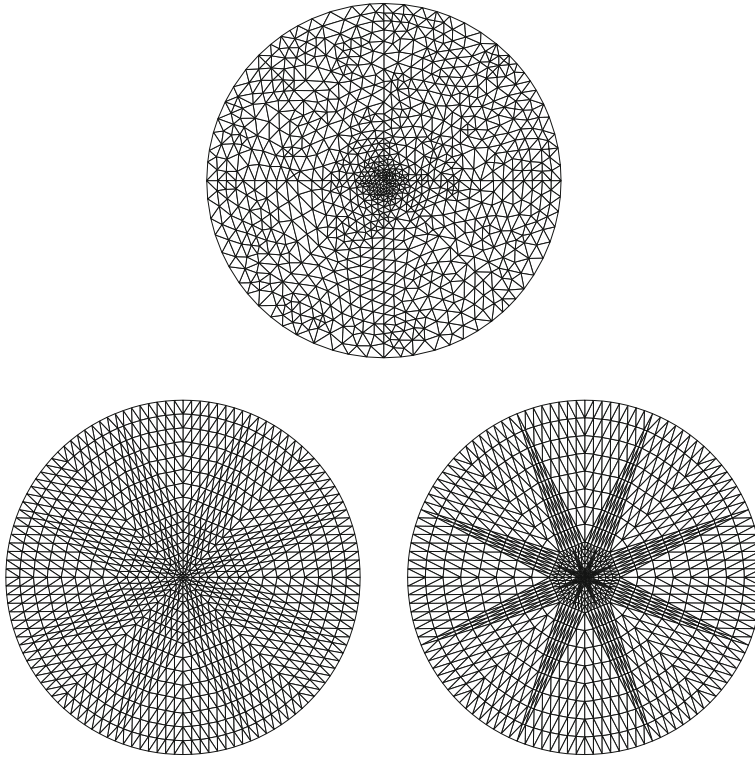


Fig. 4 Refined meshes for the unit disk, $\delta = 0.5$: adaptive refinement driven by local indicators, $N = 1,921$ (top); graded refinement with $\kappa = 0.375$, $N = 2,048$ (bottom left); graded refinement with $\kappa = 0.2$, $N = 2,048$ (bottom right)

the convergence and effectivity behavior under uniform refinement, $\kappa = 0.5$. The convergence behaviors in both norms were very similar, as before, having (least-squares) convergence models CN^{-p} for C between about 2.7 and 3.5, and p between about 0.4 and 0.41. The effectivities decreased monotonically from 1.4186 to 0.9538 for the energy norm, and from 1.4729 to 1.0228 for the H^1 semi-norm.

Although the approximate error function $\varepsilon_n \approx u - u_n$ was computed with respect to the energy inner-product B , we now demonstrate empirically that ε_n can be used to provide information about the Hessian u (recall (22)). Apart from demonstrating that more than just energy norm error can be reliably extracted from ε_n , this Hessian recovery has relevance to the discussion of the adaptive refinement employed in these experiments, as indicated in the introduction to this section.

We note that $u \in W^{2,1}(\Omega) \setminus H^2(\Omega)$, and

$$|u|_{W^{2,1}(\Omega)} = \int_{\Omega} |u_{xx}| + 2|u_{xy}| + |u_{yy}| dx \approx 16.5531.$$

All digits shown above are correct. We approximate this norm via

$$|\varepsilon_n|_{W^{2,1}(\mathcal{T}_n)} = \sum_{T \in \mathcal{T}_n} \int_T |(\varepsilon_n)_{xx}| + 2|(\varepsilon_n)_{xy}| + |(\varepsilon_n)_{yy}| dx.$$

Under each refinement scheme, the effectivity $|\varepsilon_n|_{W^{2,1}(\mathcal{T}_n)}/|u|_{W^{2,1}(\Omega)}$ improved from roughly 1.32 on the coarsest triangulation to roughly 1.00 on the finest. So we see that ε_n accurately encodes the Hessian of u . This will also be the case for the two choices of δ that follow.

When $\delta = 0.25$, our theory predicts optimal-order convergence for grading parameters $0 \leq \kappa < 0.25$. We restrict our attention to the energy norm, showing convergence histories and effectivities graphically in Fig. 5, for adaptive refinement, graded refinement with $\kappa = 0.2$, and uniform refinement ($\kappa = 0.5$). The adaptive and graded refinement schemes yield optimal-order convergence, while the convergence is clearly much worse under uniform refinement. The effectivities under each refinement scheme are generally very good, with graded refinement producing the best results. We compute $|u|_{W^{2,1}(\Omega)} \approx 19.48699$ using MATHEMATICA, and both the adaptive and graded refinement schemes approximate this value with effectivities ranging between about 1.20 on the coarsest mesh and 1.00 on the finest.

We finally consider the case $\delta = 0.0625$. Our theory predicts optimal-order convergence for grading parameters $0 \leq \kappa < 0.0625$. We restrict our attention to the energy norm, showing convergence histories and effectivities graphically in Fig. 6, for adaptive refinement, graded refinement with $\kappa = 0.06$ and uniform refinement ($\kappa = 0.5$). Also in this figure are a coarse and a modestly-refined mesh for $\kappa = 0.06$, included to illustrate that some of the triangles in these graded meshes are strongly anisotropic (needle-like). We believe that the strength of the singularity, $r^{1/4}$ near the origin, and the strongly anisotropic triangles (in the case of graded refinement) are the primary reasons for the slightly sub-optimal convergence behavior. Empirically, more refinements are needed to see the optimal convergence for strongly singular problems. The effectivities remain quite reasonable. As before, we also consider the effectivity in estimating $|u|_{W^{2,1}(\Omega)} \approx 23.37852$; for the adaptive and graded refinement schemes, the effectivities were never outside of the range $[0.90, 1.16]$ and achieved their optimal values of 1.00 and 1.01 (respectively) on their finest meshes.

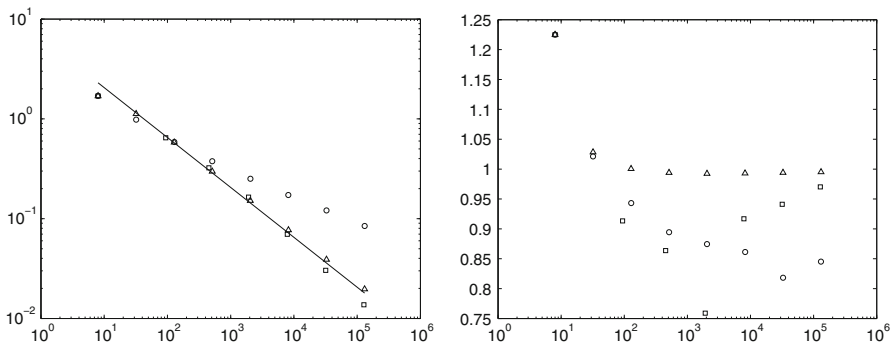


Fig. 5 Errors (left) and effectivities (right) for the unit disk in the energy norm, $\delta = 0.25$: adaptive refinement driven by local indicators (square), graded refinement with $\kappa = 0.2$ (triangle), and uniform refinement (circle). The solid line in the convergence plot has slope $-1/2$

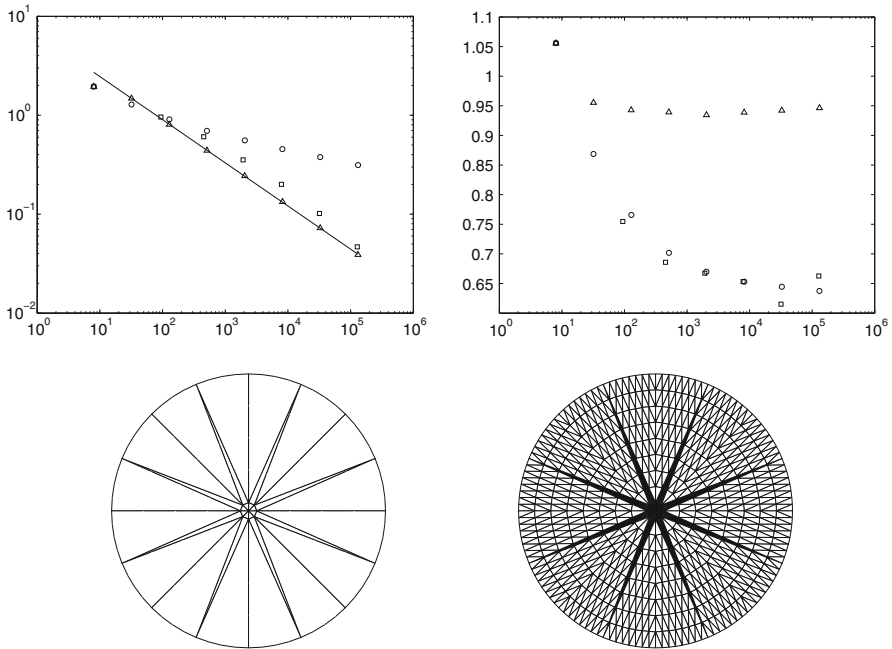


Fig. 6 Errors (top left) and effectivities (top right) for the unit disk in the energy-norm, $\delta = 0.0625$: adaptive refinement driven by local indicators (square), graded refinement with $\kappa = 0.06$ (triangle), and uniform refinement (circle). The solid line in the convergence plot has slope -0.436 . Graded meshes using $\kappa = 0.06$, $N = 32$ (bottom left) and $N = 2,048$ (bottom right)

In order to illustrate the claim that the system for computing ε_n remains well-conditioned as the mesh is refined (Theorem 3.6), we provide estimated condition numbers for both the graded meshes and adaptively refined meshes. These were computed by exporting the stiffness matrices to MATLAB and using the `eigs` command to determine the largest and smallest eigenvalues. These estimated condition numbers are given for the diagonal rescaling $B_d = D^{-1/2} B D^{-1/2}$ of the stiffness matrix B in Fig. 7. Concerning the data for graded refinement, we use $\kappa = 0.375$ for $\delta = 0.5$, $\kappa = 0.2$ for $\delta = 0.25$, and $\kappa = 0.06$ for $\delta = 0.0625$. It is clear from these graphs that the adaptively refined meshes, which produce triangles of better shape overall, yield systems with better conditioning than their graded mesh counterparts; and the condition numbers of the stiffness matrices for W_n remain bounded, while those for V_n grow linearly with the problem size.

5.2 The sector of unit disk with the singularity at the origin

For this set of experiments, we consider the sector of the unit disk (centered at the origin) for which $0 < \theta < 7\pi/4$. We impose homogeneous Dirichlet conditions on the solid portion of the boundary and homogeneous Neumann conditions on the dashed portion of the boundary—see Fig. 8. If $f = (4 - \delta - \alpha_j^2) \cos(\alpha_j \theta)$ in (2), where $\alpha_j = (4j + 2)/7$ and $j \geq 0$, then the exact solution is given by

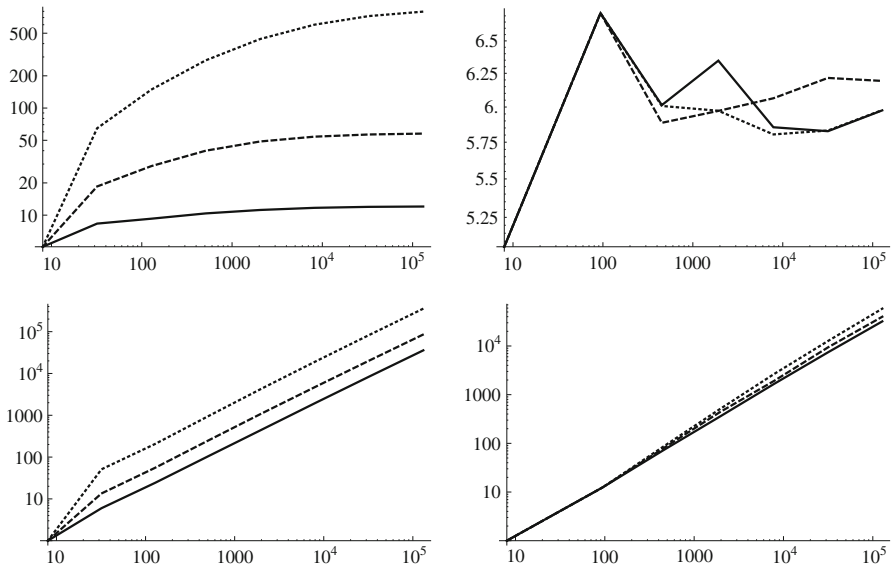


Fig. 7 Condition numbers for the Circle Problem. The *top row* provides conditioning information for the stiffness matrices on W_n , and the *bottom row* for stiffness matrices on V_n . The *left column* concerns graded refinement, and the *right column* adaptive refinement. In each case, the *solid line* corresponds to $\delta = 0.5$, the *dashed line* to $\delta = 0.25$ and the *dotted line* to $\delta = 0.0625$

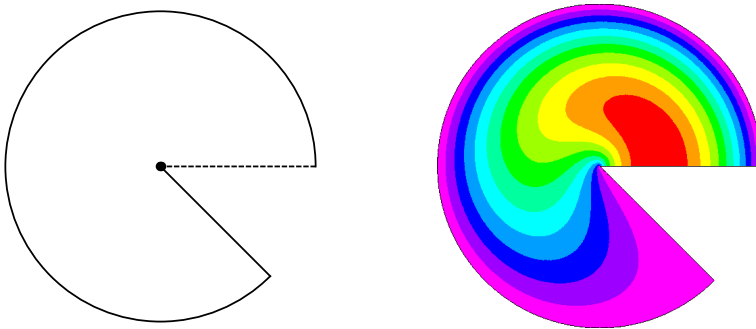


Fig. 8 Sector of the unit disk, with mixed boundary conditions (*left*), and solution when $\alpha = \alpha_0 = 2/7$ and $\delta = 1/16$

$$u = (r\sqrt{\delta + \alpha_j^2} - r^2) \cos(\alpha_j \theta).$$

We note that $v = r\sqrt{\delta + \alpha_j^2} \cos(\alpha_j \theta)$ satisfies $-\Delta v + \delta r^{-2}v = 0$ in Ω as well as the correct boundary conditions on the two straight edges of $\partial\Omega$, so this type of singular behavior is natural for the given problem. The function u was obtained from v by adding a term to give the right boundary value on the curved portion of the boundary without altering the other boundary values, while keeping the data f smooth. It is, perhaps, a bit surprising that the combination of a re-entrant corner and the r^{-2} singularity

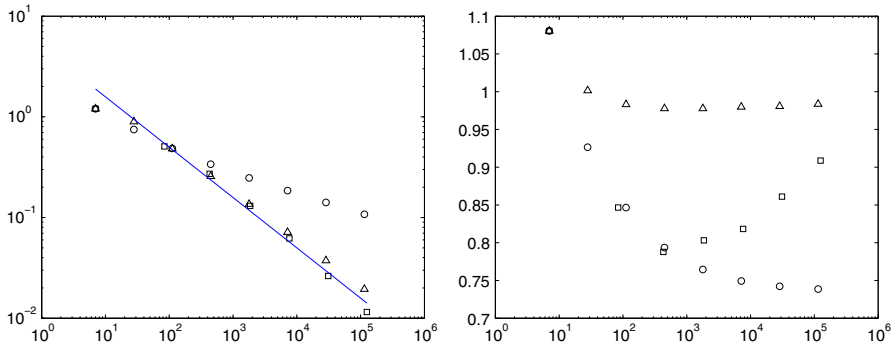


Fig. 9 Errors (*left*) and effectivities (*right*) for the sector in the energy-norm, $\delta = 0.0625$: adaptive refinement driven by local indicators (*square*), graded refinement with $\kappa = 0.15$ (*triangle*), and uniform refinement (*circle*). The *solid line* in the convergence plot has slope $-1/2$

in the operator at this corner yields a solution with higher regularity than if the r^{-2} singularity in the operator had been located elsewhere.

Because the problems are no more difficult, in terms of the singularities produced in u , than when the singular point 0 was in the interior of the domain, we only perform one experiment. Taking $\delta = 1/16 = 0.0625$ and $j = 0$, we give convergence and effectivity plots in Fig. 9 for adaptive refinement, graded refinement with $\kappa = 0.15 < 2^{-1/\eta}$ ($\eta = \sqrt{113}/28 \approx 0.379648$), and uniform refinement ($\kappa = 0.5$). The convergence rates for the adaptive and graded refinements are optimal, or nearly optimal; and the convergence rate for uniform refinement is clearly sub-optimal, as expected. Although none of the effectivities are bad, those for uniform refinement progressively deteriorate, and those for graded refinement are the best across all refinement levels.

5.3 L-shape with the singularity at the origin

Here we consider the Dirichlet problem

$$-\Delta u + \delta r^{-2}u = 1 \quad \text{in } \Omega, \quad u = 0 \text{ on } \partial\Omega$$

on the L-shaped domain pictured in Fig. 10 (together with its initial triangulation), having corners: $(-1, 1)$, $(3, -1)$, $(3, 1)$, $(1, 1)$, $(1, 3)$, $(-1, 3)$. The local regularity index at the re-entrant corner $(1,1)$ is $2/3$. At the origin, the local regularity index is $\sqrt{\delta}$, as usual. We look at the case $\delta = 0.25$, and compare adaptive, graded and uniform refinements as before, for the energy norm. For graded refinements, we employ two grading parameters, $\kappa_1 = 0.2$ for the origin, and $\kappa_2 = 0.35 < 2^{-3/2}$ for the re-entrant corner. In this case, we do not know the exact solution, so we plot only error estimates to indicate convergence histories. The previous experiments have provided sufficient evidence that these error estimates are trustworthy. The convergence plots show, as before, that some sort of adapted meshes are needed, and that both the adaptive and graded approaches yield optimal (or nearly optimal) convergence rates (Fig. 11).

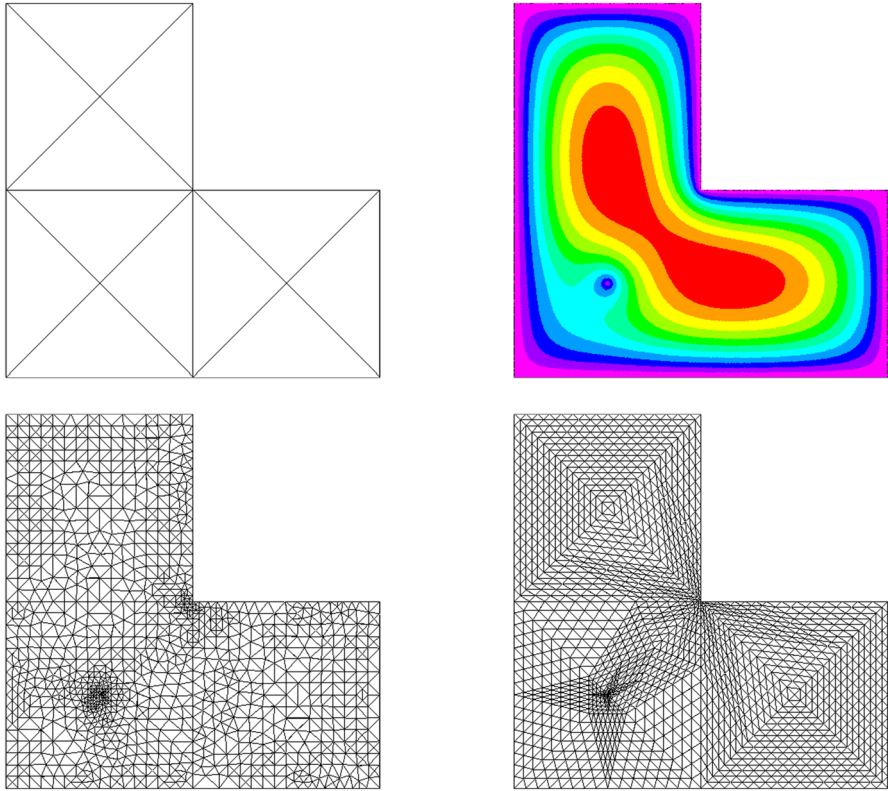
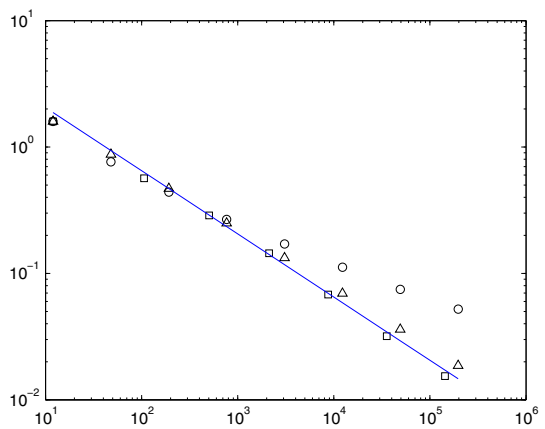


Fig. 10 On top, the L-shaped domain with initial triangulation (left), and solution when $\delta = 0.25$. At bottom, adaptive mesh with $N = 2,122$ (left), and graded mesh with $N = 3,072$

Fig. 11 Error estimates for the L-shape in the energy-norm, $\delta = 0.25$: adaptive refinement driven by local indicators (square), graded refinement (triangle), and uniform refinement (circle). In the graded refinement, two grading parameters are used: $\kappa_1 = 0.2$ at the origin, and $\kappa_2 = 0.35$ at the re-entrant corner (see Remark 3.8). The solid line in the convergence plot has slope $-1/2$



5.4 Conclusions

Our numerical tests have clearly demonstrated that the hierarchical error estimate provides both efficient and reliable error information in the energy and H^1 norms, with effectivities very close to one at all levels of refinement. In terms of convergence rates and effectivities, there was no clear winner between graded meshes and the adaptively refined ones. Adaptively refined meshes clearly outperform their graded counterparts in terms of the condition numbers of the stiffness matrices for the spaces V_n and W_n , due to the generation of triangles with no extreme angles. However, we reiterate that our theoretical results asserting optimal convergence rates and the asymptotic equivalence of error and error estimate are proved only in the graded mesh setting. To obtain analogous convergence results for adaptively refined meshes is challenging even for much simpler problems posed in H^1 , though the basic framework for proofs in that context is well-developed at this stage [18, 23, 38, 42, 49]. We note that, even in this simpler setting, proofs of convergence for adaptivity driven by hierarchical error estimates of the type put forth here have not yet been obtained—the paper [38] proves adaptive convergence based on “hierarchical estimators”, but they use this term for an explicit error estimate much like that of standard residual estimates, following terminology used in [50] as opposed to [2, 8].

Acknowledgments The authors thank Dr. Alan Demlow for helpful remarks concerning Lemma 4.3.

References

1. Adams, R.A., Fournier, J.J.F.: Sobolev Spaces. Pure and Applied Mathematics, vol. 140, 2nd edn. Elsevier/Academic Press, Amsterdam (2003)
2. Ainsworth, M., Oden, J.T.: A Posteriori Error Estimation in Finite Element Analysis. Pure and Applied Mathematics. Wiley-Interscience, New York (2000)
3. Apel, T., Nicaise, S.: The finite element method with anisotropic mesh grading for elliptic problems in domains with corners and edges. *Math. Methods Appl. Sci.* **21**(6), 519–549 (1998)
4. Araya, R., Poza, A.H., Stephan, E.P.: A hierarchical a posteriori error estimate for an advection-diffusion-reaction problem. *Math. Models Methods Appl. Sci.* **15**(7), 1119–1139 (2005)
5. Babuška, I., Kellogg, R.B., Pitkäranta, J.: Direct and inverse error estimates for finite elements with mesh refinements. *Numer. Math.* **33**(4), 447–471 (1979)
6. Băcuță, C., Nistor, V., Zikatanov, L.: Improving the rate of convergence of high-order finite elements on polyhedra. I. A priori estimates. *Numer. Funct. Anal. Optim.* **26**(6), 613–639 (2005)
7. Băcuță, C., Nistor, V., Zikatanov, L.T.: Improving the rate of convergence of ‘high order finite elements’ on polygons and domains with cusps. *Numer. Math.* **100**(2), 165–184 (2005)
8. Bank, R.E.: Hierarchical Bases and the Finite Element Method. *Acta Numerica*, vol. 5. Cambridge University Press, Cambridge (1996)
9. Bank, R.E.: PLTMG: A software package for solving elliptic partial differential equations. Users’ Guide 10.0. Technical report, University of California at San Diego, Department of Mathematics (2007)
10. Bank, R.E., Grubišić, L., Owall, J.S.: A framework for robust eigenvalue and eigenvector error estimation and Ritz value convergence enhancement. *Appl. Numer. Math.* **66**, 1–29 (2013)
11. Bank, R.E., Smith, R.K.: A posteriori error estimates based on hierarchical bases. *SIAM J. Numer. Anal.* **30**(4), 921–935 (1993)
12. Bank, R.E., Smith, R.K.: Mesh smoothing using a posteriori error estimates. *SIAM J. Numer. Anal.* **34**(3), 979–997 (1997)
13. Bank, R.E., Smith, R.K.: An algebraic multilevel multigraph algorithm. *SIAM J. Sci. Comput.* **23**(5), 1572–1592 (2002). (electronic)

14. Bank, R.E., Xu, J.: Asymptotically exact a posteriori error estimators. II. General unstructured grids. *SIAM J. Numer. Anal.* **41**(6), 2313–2332 (2003). (electronic)
15. Bornemann, F.A., Erdmann, B., Kornhuber, R.: A posteriori error estimates for elliptic problems in two and three space dimensions. *SIAM J. Numer. Anal.* **33**(3), 1188–1204 (1996)
16. Brenner, S., Cui, J., Gudi, T., Sung, L.-Y.: Multigrid algorithms for symmetric discontinuous Galerkin methods on graded meshes. *Numer. Math.* **119**(1), 21–47 (2011)
17. Brenner, S., Cui, J., Sung, L.-Y.: Multigrid methods for the symmetric interior penalty method on graded meshes. *Numer. Linear Algebra Appl.* **16**(6), 481–501 (2009)
18. Cascon, J.M., Kreuzer, C., Nochetto, R.H., Siebert, K.G.: Quasi-optimal convergence rate for an adaptive finite element method. *SIAM J. Numer. Anal.* **46**(5), 2524–2550 (2008)
19. Chen, L., Li, H.: Superconvergence of gradient recovery schemes on graded meshes for corner singularities. *J. Comput. Math.* **28**(1), 11–31 (2010)
20. Chen, L., Xu, J.: A posteriori error estimator by post-processing. In: Tang, T., Xu, J. (eds.) *Adaptive Computations: Theory and Algorithms*. Mathematics Monographs, Series 6. Science Press, Beijing (2007)
21. Dauge, M.: *Elliptic Boundary Value Problems on Corner Domains*. Lecture Notes in Mathematics, vol. 1341. Springer, Berlin (1988)
22. Deuffhard, P., Leinen, P., Yserentant, H.: Concepts of an adaptive hierarchical finite element code. *IMPACT Comput. Sci. Eng.* **1**(1), 3–35 (1989)
23. Dörfler, W.: A convergent adaptive algorithm for Poisson’s equation. *SIAM J. Numer. Anal.* **33**(3), 1106–1124 (1996)
24. Dupont, T., Scott, R.: Polynomial approximation of functions in Sobolev spaces. *Math. Comput.* **34**(150), 441–463 (1980)
25. Felli, V., Ferrero, A., Terracini, S.: Asymptotic behavior of solutions to Schrödinger equations near an isolated singularity of the electromagnetic potential. *J. Eur. Math. Soc. (JEMS)* **13**(1), 119–174 (2011)
26. Felli, V., Marchini, E., Terracini, S.: On the behavior of solutions to Schrödinger equations with dipole type potentials near the singularity. *Discrete Contin. Dyn. Syst.* **21**(1), 91–119 (2008)
27. Fournais, S., Hoffmann-Ostenhof, M., Hoffmann-Ostenhof, T., Østergaard, T., Sørensen. Analytic structure of solutions to multiconfiguration equations. *J. Phys. A* **42**(31):315208 (2009)
28. Grisvard, P.: *Elliptic problems in nonsmooth domains*, Monographs and Studies in Mathematics, vol. 24. Pitman (Advanced Publishing Program), Boston (1985)
29. Grisvard, P.: *Singularities in boundary value problems*, *Recherches en Mathématiques Appliquées [Research in Applied Mathematics]*, vol. 22. Masson, Paris (1992)
30. Grubišić, L., Ovall, J.S.: On estimators for eigenvalue/eigenvector approximations. *Math. Comput.* **78**, 739–770 (2009)
31. Holst, M., Ovall, J.S., Szypowski, R.: An efficient, reliable and robust error estimator for elliptic problems in \mathbb{R}^3 . *Appl. Numer. Math.* **61**(5), 675–695 (2011)
32. Hunsicker, E., Li, H., Nistor, V., Ville, U.: Analysis of Schrödinger operators with inverse square potentials I: regularity results in 3D. *Bull. Math. Soc. Sci. Math. Roumanie (N.S.)* **55**(103):157–178 (2012)
33. Hunsicker, E., Li, H., Nistor, V., Ville, U.: Analysis of Schrödinger operators with inverse square potentials II: FEM and approximation of eigenfunctions in the periodic case (2012, submitted)
34. Key, K., Ovall, J.: A parallel goal-oriented adaptive finite element method for 2.5-d electromagnetic modelling. *Geophys. J. Int.* **186**(1), 137–154 (2011)
35. Kondrat’ev, V.A.: Boundary value problems for elliptic equations in domains with conical or angular points. *Trudy Moskov. Mat. Obšč.* **16**, 209–292 (1967)
36. Kozlov, V.A., Maz’ya, V.G., Rossmann, J.: *Elliptic boundary value problems in domains with point singularities*, *Mathematical Surveys and Monographs*, vol. 52. American Mathematical Society, Providence (1997)
37. Kozlov, V.A., Maz’ya, V.G., Rossmann, J.: *Spectral problems associated with corner singularities of solutions to elliptic equations*, *Mathematical Surveys and Monographs*, vol. 85. American Mathematical Society, Providence (2001)
38. Kreuzer, C., Siebert, K.G.: Decay rates of adaptive finite elements with Dörfler marking. *Numer. Math.* <http://www.springerlink.com/content/86108538130mq17/> (2010)
39. Li, H.: Finite element analysis for the axisymmetric Laplace operator on polygonal domains. *J. Comput. Appl. Math.* **235**, 5155–5176 (2011)

40. Li, H., Mazzucato, A., Nistor, V.: Analysis of the finite element method for transmission/mixed boundary value problems on general polygonal domains. *Electron. Trans. Numer. Anal.* **37**, 41–69 (2010)
41. Li, H., Nistor, V.: Analysis of a modified Schrödinger operator in 2D: regularity, index, and FEM. *J. Comput. Appl. Math.* **224**(1), 320–338 (2009)
42. Morin, P., Nochetto, R.H., Siebert, K.G.: Convergence of adaptive finite element methods. *SIAM Rev.* **44**(4), 631–658 (electronic) (2003) [Revised reprint of Data oscillation and convergence of adaptive FEM. *SIAM J. Numer. Anal.* **38**(2), 466–488 (2000) (electronic); MR1770058 (2001g:65157)]
43. Moroz, S., Schmidt, R.: Nonrelativistic inverse square potential, scale anomaly, and complex extension. Preprint hep-th/0909.3477v3 (2010)
44. Owall, J.S.: Asymptotically exact functional error estimators based on superconvergent gradient recovery. *Numer. Math.* **102**(3), 543–558 (2006)
45. Owall, J.S.: Function, gradient, and Hessian recovery using quadratic edge-bump functions. *SIAM J. Numer. Anal.* **45**(3), 1064–1080 (2007). (electronic)
46. Raugel, G.: Résolution numérique par une méthode d'éléments finis du problème de Dirichlet pour le laplacien dans un polygone. *C. R. Acad. Sci. Paris Sér. A-B* **286**(18), A791–A794 (1978)
47. Rivara, M.-C.: New longest-edge algorithms for the refinement and/or improvement of unstructured triangulations. *Int. J. Numer. Methods Eng.* **40**(18), 3313–3324 (1997)
48. Schatz, A.H., Sloan, I.H., Wahlbin, L.B.: Superconvergence in finite element methods and meshes that are locally symmetric with respect to a point. *SIAM J. Numer. Anal.* **33**(2), 505–521 (1996)
49. Stevenson, R.: Optimality of a standard adaptive finite element method. *Found. Comput. Math.* **7**(2), 245–269 (2007)
50. Verfürth, R.: A review of a posteriori error estimation and adaptive mesh-refinement techniques. Wiley-Teubner, New York (1996)
51. Wigley, N.M.: Asymptotic expansions at a corner of solutions of mixed boundary value problems. *J. Math. Mech.* **13**, 549–576 (1964)
52. Wu, H., Sprung, D.: Inverse-square potential and the quantum vortex. *Phys. Rev. A* **49**, 4305–4311 (1994)
53. Xu, J., Zhang, Z.: Analysis of recovery type a posteriori error estimators for mildly structured grids. *Math. Comput.* **73**(247), 1139–1152 (2004). (electronic)